Correlated electron states and transport in triangular arrays

D. S. Novikov,[1,2,*] B. Kozinsky,[1] and L. S. Levitov[1]
[1]*Center for Materials Science and Engineering, Physics Department, Massachusetts Institute of Technology, 77 Massachusetts Avenue, Cambridge, Massachusetts 02139, USA*
[2]*Department of Electrical Engineering and Department of Physics, Princeton University, Princeton, New Jersey 08544, USA*
(Received 19 November 2001; published 27 December 2005)

We study correlated electron states in frustrated geometry of a triangular lattice. The interplay of long-range interactions and finite residual entropy of a classical system gives rise to unusual effects in equilibrium ordering as well as in transport. A correlated fluid phase is identified in a wide range of densities and temperatures above freezing into commensurate solid phases. The charge dynamics in the correlated phase is described in terms of a height field, its fluctuations, and topological defects. We demonstrate that the height field fluctuations give rise to a "free" charge flow and finite dc conductivity. We show that freezing into the solid phase, controlled by the long-range interactions, manifests itself in singularities of transport properties.

DOI: 10.1103/PhysRevB.72.235331 PACS number(s): 73.61.−r, 73.50.−h

I. INTRODUCTION

The properties of geometrically frustrated systems are complex due to the presence of an energy landscape with many degenerate or nearly degenerate minima.[1] These systems exhibit qualitatively new effects, such as an extensive ground state degeneracy and suppression of freezing down to zero temperature. The latter phenomena traditionally have been studied in the context of antiferromagnetic spin models on appropriately chosen lattices, and other models with short-range interactions.

Below we demonstrate that similar effects of geometrical frustration can naturally arise in a classical charge system. Namely, we consider ordering and dynamics of classical electrons on a triangular lattice with repulsive Coulomb interaction between charges on different lattice sites. The frustration reveals itself in the phase diagram, and also makes charge dynamics and transport very unusual. Here we focus on the electric transport as a natural means to study ordering types and phase transitions in a charge system.

Two-dimensional frustrated lattices arise in a variety of experimental systems. Artificial structures, such as Josephson junction arrays[2] and arrays of quantum dots,[3] have recently become available. One attractive feature of these systems is the control of the Hamiltonian and, in particular, of frustration, by the system design. Also, experimental techniques available for probing magnetic flux or charge ordering, such as electric transport measurements and scanning probes, are more diverse and flexible than those conventionally used to study magnetic or structural ordering in solids. There have been extensive theoretical[4,5] and experimental[2] studies of phase transitions and collective phenomena in Josephson arrays. Another example of frustrated charge systems is provided by recently discovered superconducting materials based on CoO_2.[6]

In the present work we discuss a realization of a frustrated charge system in a two-dimensional (2D) triangular array of quantum dots. Recent progress in the epitaxial and lithographic techniques made it possible to produce[3] regular and irregular arrays of quantum dots, in which the size of an individual dot can be tuned in the 10–100 nm range with the rms size distribution of 10%–20%. Such arrays are made of InAs or Ge islands embedded into the semiconductor substrate. This stimulated experimental[7] and theoretical[8] investigation of electronic ordering and transport in these arrays. Capacitance and conductivity measurements[7] show the quantized nature of charging of the dots. However, the interdot Coulomb interaction in such systems is weak compared to the individual dot charging energy as well as potential fluctuations due to disorder in the substrate.

A promising system fabricated and studied recently[9] involves nanocrystallite quantum dots which are synthesized with high reproducibility, of diameters $\sim 1.5-15$ nm tunable during synthesis, with a narrow size distribution (within 5% rms). These dots can be forced to assemble into ordered three-dimensional (3D) closely packed colloidal crystals,[9] with the structure of stacked 2D triangular lattices. High flexibility and structural control open a possibility to study effects inaccessible in the more traditional self-assembled quantum dot arrays fabricated using epitaxial growth techniques. In particular, the high charging energy that can reach or exceed the room temperature scale, and the triangular lattice geometry of the dot arrays[9] are of interest from the point of view of exploring aspects of charge ordering and transport.[10,11]

From a theoretical viewpoint, charge ordering is closely related to, or can be interpreted in terms of, a suitably chosen spin system. Spin models, which serve as a paradigm in a theory of critical phenomena, have applications to ordering in different systems, such as the phase transitions in adsorbed monolayers.[12] In our analysis we map the charge problem onto the triangular antiferromagnetic Ising spin problem. In the situation of interest, when charging energy enforces single or zero occupancy of the sites, one can interpret the occupied and unoccupied dots as an up spin and down spin states. Since the like charges repel, the corresponding effective spin interaction is indeed of an antiferromagnetic kind. Appropriately, charge density plays the role of spin density, and the gate voltage corresponds to an external magnetic field. Besides, one can map the offset charge disorder (random potentials on the dots) onto a random magnetic field in the spin problem.

There are, however, a few theoretical and experimental aspects of the charge-spin mapping that make the two problems not entirely equivalent. First, charge conservation in the electron problem gives rise to a constraint on total spin in the associated spin problem. This leads to a dynamical constraint, namely blocking of single spin flips. Microscopically, spin conservation requires the Kawasaki (or type B) dynamics[13] as opposed to the nonconserving Glauber (or type A) dynamics.[14] This makes no difference with regard to the thermodynamic state at equilibrium, since the system with fixed total spin is statistically equivalent to the grand canonical ensemble. However, the order parameter conservation manifests itself both in a slower dynamics[15] and in collective transport properties of the correlated fluid phase discussed below.

Another important difference between the charge and spin problems is in the form of interaction. Spin systems are usually described by a nearest neighbor interaction. In the spin problem relevant for this work, the triangular Ising antiferromagnet (ΔIAFM) with the nearest neighbor interaction, an exact solution in zero field has been obtained by Wannier[16] who demonstrated that there is no ordering phase transition at any finite temperature. In contrast, in the charge problem studied in this paper the long-range Coulomb interaction makes the phase diagram more rich. We find phase transitions at finite temperature for certain charge densities.

One of the main objects in our focus is the correlated fluid phase, that arises at relatively low temperatures due to geometric frustration preventing freezing. In this phase, equilibrium fluctuations and transport exhibit strong correlations. We employ a nonlocal description in terms of the height field, used earlier in spin models,[17,18] to map charge dynamics onto Gaussian fluctuations of the height surface in the presence of topological defects (dislocations). We find that both the height field fluctuations and the presence of defects contribute to low-temperature transport properties.

The outline of the paper is as follows. In Sec. II a charge Hamiltonian is introduced and stochastic Monte Carlo (MC) dynamics is defined, based on the correspondence between the charges and Ising spins. The MC dynamics is used to obtain the phase diagram (Sec. III) and to study the dc conductivity as a function of temperature and electron density (Sec. IV).

In Sec. V a height field-order parameter is defined and used to describe the charge ordering. In Sec. VI we compare the contributions to transport due to the height surface fluctuations and the topological defects. Subsequently, in Sec. VII, we study the height variable fluctuations and evaluate their effective stiffness from the MC dynamics. By comparing the stiffness to the universal value we rule out the Berezinskii-Kosterlitz-Thouless transition and prove that the defects are always unbound. In Sec. VIII we present scaling arguments that support the conclusions of Sec. VII, and set bounds on the height surface stiffness. In Sec. IX we consider dynamical fluctuations of the height variable and estimate their effect on dc conductivity.

II. THE MODEL

The Hamiltonian $\mathcal{H}_{\rm el}$ of a quantum dot array describes charges q_i on the dots, their Coulomb interaction as well as coupling to the background disorder potential $\phi(\mathbf{r})$ and to the gate potential V_g,

$$\mathcal{H}_{\rm el}=\frac{1}{2}\sum_{i,j}V(\mathbf{r}_{ij})q_iq_j+\sum_{\mathbf{r}_i}[V_g+\phi(\mathbf{r}_i)]q_i. \tag{1}$$

Here the vectors $\mathbf{r}_i$ run over a triangular lattice with the lattice constant a, and $\mathbf{r}_{ij}=\mathbf{r}_i-\mathbf{r}_j$. The interaction $V(\mathbf{r})$ includes a term describing screening by the gate,

$$V(\mathbf{r}_{ij}\neq 0)=\left(\frac{e^2}{\epsilon|\mathbf{r}_{ij}|}-\frac{e^2}{\epsilon\sqrt{(\mathbf{r}_{ij})^2+d^2}}\right)e^{-\gamma|\mathbf{r}_{ij}|}. \tag{2}$$

Here ϵ is the dielectric constant of the substrate, and $d/2$ is the distance to the gate plane. [The parameter d in (2) which controls the interaction range is chosen in our simulation in the interval $0\leqslant d/2\leqslant 5a$.] The single dot charging energy $\frac{1}{2}V(0)=e^2/2C$ is assumed to be large enough to inhibit multiple occupancy, so that $q_i=0,1$.

The exponential factor in (2) is introduced for convenience, to control convergence of the sum in (1). Below we use $\gamma^{-1}=2d$. In the case of spatially varying ϵ the form of interaction can be more complicated. For example, for an array of dots on a dielectric substrate, one should replace ϵ in Eq. (2) by $(\epsilon+1)/2$.

Electron tunneling in the system[9–11] presumably occurs mainly between neighboring dots. The tunneling is probably incoherent, i.e., assisted by some energy relaxation mechanism, such as phonons. Since the tunneling coupling of the dots is weak,[9–11] we focus on the charge states and ignore the effects of electron spin, such as exchange, spin ordering, etc.

The incoherent nature of electron hopping warrants employing stochastic MC dynamics in which transitions between different states take place in accordance with Boltzmann probabilities. The states undergoing the MC dynamics are charge configurations with $q_i=0,1$ on a $N\times N$ patch of a triangular array. Periodic boundary conditions are imposed by extending the $N\times N$ configurations q_i along with the Hamiltonian (1) periodically over the entire plane. Spatial periodicity of the MC dynamics is maintained by allowing charge hops across the boundary, so that the charges disappearing on one side of the patch reappear on the opposite side.

Charge conservation gives a constraint $\Sigma q_i=$const that must be enforced throughout the MC evolution. While contributing to MC dynamics slowing down, this constraint has no effect on the statistical equilibrium and the thermodynamic properties. To study ordering one can employ the nonconserving A dynamics, with the gate voltage V_g serving as a parameter controlling the system state. This is beneficial due to relatively high speed of the A dynamics. In turn, the somewhat slower charge conserving B dynamics is used to investigate conductivity at fixed charge density

$$n=A^{-1}\sum_i q_i,\quad A=N^2. \tag{3}$$

Below we recall the definition of the dynamics A and B, and introduce the charge-spin mapping which will be used throughout the paper.

A. The dynamics of type *A*

In the MC dynamics of type A, since charge is not conserved, the charge state is updated independently on different sites. The occupancy of a randomly selected site i is changed or preserved with the probabilities W_i and $\bar{W}_i$, which depend on the system state and its attempted change as follows:

$$W_i/\bar{W}_i = \exp(-\delta E_i^{(A)}/T_{\rm el}), \tag{4}$$

$$\delta E_i^{(A)} = \delta q_i \Phi_i, \tag{5}$$

where $W_i+\bar{W}_i=1$. Here δq_i is the attempted change of the charge at the site i, whereby the potential is

$$\Phi_i = \sum_{r_j \neq r_i} V(\mathbf{r}_{ij}) q_j + V_g + \phi(\mathbf{r}_i), \tag{6}$$

and $T_{\rm el}$ is the temperature in the charge system (for brevity, from now on we set $k_B \equiv 1$). At each MC time step, the charge configuration is affected only on one site. The potential Φ_i at this site is obtained using the current system state modified at the preceding MC step.

B. The dynamics of type *B*

To enforce charge conservation appropriate for the B dynamics, we update the state of the system by exchanging charges on randomly chosen neighboring sites. Specifically, we randomly select a site i. Then, at each MC time step, we randomly chose a site j neighboring to i until the occupancy of the sites i and j are not the same, $q_j \neq q_i$. After that, the occupancies of the sites i and j are exchanged with probability $W_{i\to j}$, and remain unchanged with probability $W_{i\to i}$, such that

$$W_{i\to j}/W_{i\to i} = \exp(-\delta E_{ij}^{(B)}/T_{\rm el}), \tag{7}$$

$$\delta E_{ij}^{(B)} = (q_j - q_i)(\Phi_i - \Phi_j) - (q_j - q_i)^2 V(\mathbf{r}_{ij}), \tag{8}$$

where $W_{i\to j}+W_{i\to i}=1$, and the potential Φ_i is defined by Eq. (6).

C. Charge-spin mapping

The model (1), (2), (4), and (7) possesses an electron-hole symmetry, exhibited by introducing a spin variable

$$s_i = 2q_i - 1 = \pm 1. \tag{9}$$

The charge Hamiltonian (1), rewritten in terms of the spin variables (9), becomes

$$\mathcal{H}_{\rm el} = \tfrac{1}{4}\mathcal{H}_s + \text{const}, \tag{10}$$

$$\mathcal{H}_s = \frac{1}{2}\sum_{i,j} V(\mathbf{r}_{ij}) s_i s_j + \sum_{\mathbf{r}_i} [\mu + 2\phi(\mathbf{r}_i)] s_i. \tag{11}$$

Here we introduced the chemical potential,

$$\mu = 2V_g + V_{\mathbf{k}=0} \tag{12}$$

that corresponds to an external field for the spins s_i. Here $V_{\mathbf{k}} = \Sigma_j e^{-i\mathbf{r}_j\mathbf{k}} V(\mathbf{r}_j)$ is the Fourier transform of the interaction (2). In terms of spin variables the charge density (3) is given by

$$n = A^{-1}\sum_i \frac{1}{2}(s_i + 1), \quad A = N^2. \tag{13}$$

In the corresponding stochastic dynamics for the spin system, defined as above, we use s_i instead of q_i in the energies (5) and (8), and rescale $T_{\rm el}$ to the spin temperature,

$$T = 4T_{\rm el}. \tag{14}$$

Equations (9)–(14) provide a mapping of the charge problem onto a spin system with long-range interaction (2). The positive sign of the coupling (2) corresponds to antiferromagnetic nearest neighbor interaction. We note that the limit $d \ll a$ corresponds to the ΔIAFM problem[16–18] with nearest neighbor interaction. Unless explicitly stated, below we consider a system without disorder, $\phi(\mathbf{r})=0$.

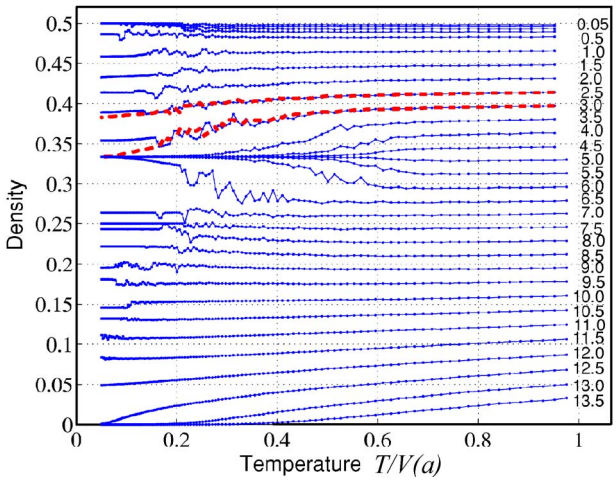

FIG. 1. (Color online) Cooling curves $n(T)$ at fixed gate voltage V_g for the screening length parameter $d=2a$. Due to the electron-hole symmetry, only the densities $0 \leqslant n \leqslant 1/2$ are shown. The values of μ, related to V_g via (12), are given on the right-hand side of the plot. Not labeled are the curves with $\mu=0.1, 0.2, 0.3$ converging to $n=1/2$. Additional cooldowns are shown for $\mu=2.5$ and $\mu=3.0$ (dashed line).

III. PHASE DIAGRAM

A. Cooling curves

To explore the ground states as a function of the chemical potential μ, we use the type A (nonconserving) MC dynamics. To reach the true equilibrium at low temperatures the usual precautions are taken by running MC first at an elevated temperature, and then gradually decreasing it to the desired value.

The cooling curves in Fig. 1 show the temperature dependence of electron density $n(T)$ for a moderate value of the screening length $d=2a$, with the temperature T measured in units of the nearest neighbor coupling $V(a)$. Due to the electron-hole symmetry $n \leftrightarrow 1-n$, it suffices to consider only $0 \leqslant n \leqslant 1/2$. Similar curves obtained for the ΔIAFM problem

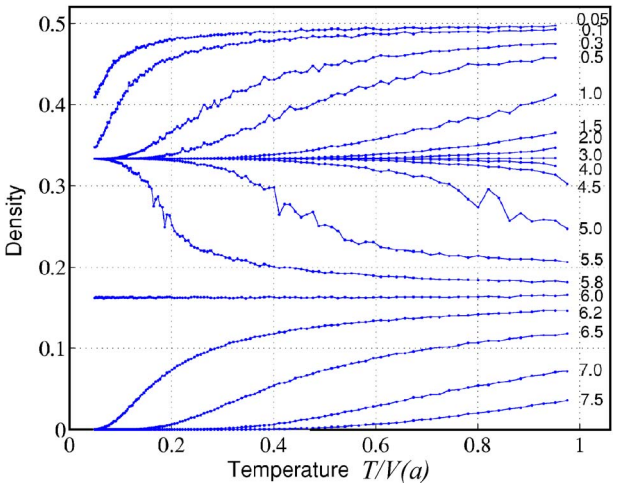

FIG. 2. (Color online) A family of cooling curves obtained in the same way as in Fig. 1 for $d \ll a$ (the pure ΔIAFM case). The values of μ are given on the right-hand side.

realized at small $d \ll a$ are displayed in Fig. 2.

The two families of cooling curves are qualitatively similar in the character of temperature dependence, slow at high T, faster at lower T, and exhibiting strong fluctuations before final stabilization at the $T=0$ value. Also, in both cases the trajectories are attracted to the densities $n=0,1$ and $n=1/3,2/3$. We note, however, qualitatively new features in the case of long range interaction (Fig. 1). The most obvious one is that the values of n attained at $T \to 0$ span a range of intermediate densities, with n being a continuous function of V_g. This behavior, indicating freezing transitions at all density values, should be contrasted with the $T \to 0$ behavior in the ΔIAFM case, characterized by discontinuous jumps between $n=0,1/3,2/3,1$. The latter four values correspond to the incompressible states (plateaus in the dependence of n vs V_g).

The long-range interactions give rise to ordering at the densities not realized in the ΔIAFM problem, the simple fraction $n=1/2$ being the most prominent one (Fig. 1). This density is an attractor for a family of cooling curves at $|\mu| \lesssim 0.5$. Several such curves, obtained for $\mu=0.05,0.1,0.2,0.3$, are shown in the top part of Fig. 1. Evidently, the basin of attraction of the $n=1/2$ state is considerably smaller than that of the $n=1/3$ and $n=2/3$ states, which is to be expected, since the ordering at $n=1/2$ is controlled by the next-to-nearest neighbor interactions.

The result of cooling, in general, is found to depend somewhat on the cooling history, especially near the incompressible densities. For different initial random distributions of charge, and depending on the specific sequence of MC moves, MC relaxation can lead to different ground states. This happens because for a generic long-range interaction there are many states nearly degenerate in energy, as illustrated in Fig. 1 by the two pairs of curves starting at $\mu=2.5$ and $\mu=3.0$ obtained for different runs of the MC dynamics. These curves, identical at high T, diverge below the temperature interval where fluctuations develop. The dependence on the cooling history in the fluctuation region limits the accuracy of phase diagram obtained from cooling trajectories in a finite system.

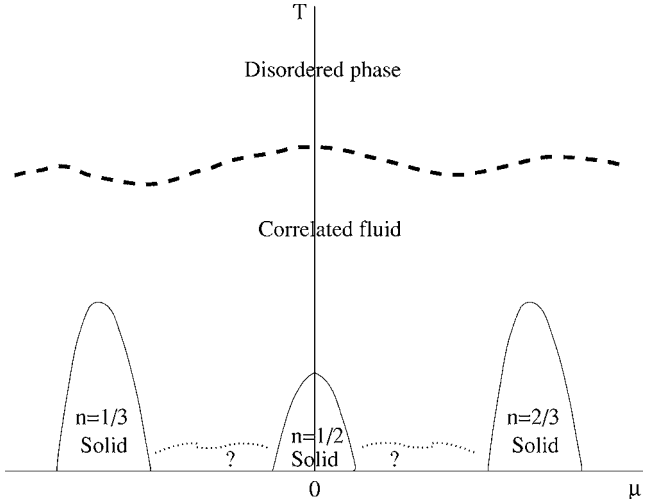

FIG. 3. Schematic phase diagram on the (μ,T) plane for a generic value of the screening length parameter $d>0$. The dashed line marks the crossover between the correlated fluid and the disordered phase. The low temperature phases denoted by a question mark could be either commensurate or disordered.

Figure 3 summarizes in a schematic way the results of the MC study of cooling. It shows the phase diagram of the system in the (μ,T) plane. Due to the particle-hole equivalence, it posesses the $\mu \leftrightarrow -\mu$ symmetry. For a generic value of the chemical potential we find three distinct temperature phases: (i) the disordered state at high temperature, (ii) the correlated fluid phase at intermediate temperatures, and (iii) the solid phases at low T.

B. Freezing transitions

Ordering at different n resembles, and indeed can be connected to, the phase transitions in adsorbed monolayers.[12] The latter have been mapped on the known statistical models (Ising, Potts, etc.), some of which are exactly solvable.[19] Possible phase transitions in 2D have been classified by Domany *et al.*[20] and by Rottman[21] based on the Landau theory.[22]

The new ingredient in the charge system, the long-range interaction, does not change the symmetry of the Landau free energy.[20,21] Still, the long-range interaction can, in principle, change the order of the transition if the latter is dominated by fluctuations, making it deviate from the Landau theory scenario. While determining the specifics of the freezing transitions in this more general case is beyond the scope of the present work, one can make the following observations.

(i) At the densities $n=1/3,2/3$, freezing occurs into one of the three degenerate $\sqrt{3}\times\sqrt{3}$ configurations [see Fig. 6(a) below]. In this state, electrons can occupy one out of the three sublattices of the triangular lattice. We believe that this transition is of the first order. Our argument is based on the steplike singularity of the average energy of the system at the transition observed during the MC dynamics,[23] and is corroborated by a fairly sharp steplike singularity in the MC conductivity (see below, Sec. IV), interpreted using the general connection of the singularities in conductivity and in

average energy.[15] Besides, for this transition a cubic invariant in the Landau free energy is allowed.[20,21,23]

An alternative scenario for freezing at this density is a continuous transition of the $q=3$ Potts universality class.[20,21] This possibility, in principle, cannot be ruled out based just on symmetry, since in two dimensions there are exceptions from the Landau theory, notably the $q=3,4$ Potts models, for which the transition is second-order even though the cubic invariants exist.[19] We believe, however, that in the present case the existence of the cubic invariant triggers the first order transition. We also note that the experimental evidence for adsorbtion of nitrogen molecules on graphite does not contradict the first-order transition scenario[24] even for fairly short-ranged quadrupolar molecular interactions.

(ii) At the density $n=1/2$, the ground state is a (2×1) charge density wave of three possible orientations [see Fig. 6(c)]. In the ordered state electrons occupy one out of the two sublattices, resulting in the sixfold degeneracy of the ground state.

The nature of the phase transition for $n=1/2$ is less clear. The classification[20,21] suggests the $q=4$ Potts universality class with a second-order transition. However, the electron-hole symmetry at the $\mu=0$ line forbids the cubic invariant in the corresponding Landau free energy, placing this transition into the universality class of the Heisenberg model with cubic anisotropy.[25] The transition in the latter model is still poorly understood,[26] with both the continuous and the fluctuation-induced first-order transition on the table.[27] Recent study[28] of the zero-field ΔIAFM with finite-range interactions (beyond the nearest-neighbor) generally favors the first-order transition, while leaving room for an additional continuous transition at special values of couplings. At $\mu\neq0$, in the absence of electron-hole symmetry, the presence of the cubic invariant makes the first-order transition scenario even more likely.

Our numerical accuracy does not allow us to make a definite prediction. The observed kink in the conductivity (Sec. IV below) is consistent with either the first- or the second-order transition, as is the singularity in the average energy.[23] In general, freezing transition into the $n=1/2$ ground state is less pronounced than that for $n=1/3,2/3$ states, since it is determined by the next-to-nearest neighbor coupling.

(iii) For a generic density n we observe that at decreasing T the MC dynamics slows down, and all the charges eventually become immobile. The ground state in general looks disordered, and depends somewhat on the cooling history. The system configuration space appears to have many nearly degenerate minima, which complicates finding the true ground state numerically. While a disordered ground state for a continuous range of densities cannot be ruled out, we anticipate freezing into commensurate "epitaxial solids" for at least some rational densities $n=p/q$ with higher denominators, such as the striped ground state for the density $n=3/7$ shown in Fig. 6(d). These transitions would take place at ever smaller temperatures since they are governed by the couplings $V(\mathbf{r})$ beyond nearest and next-to-nearest. For instance, for our model interaction (2) with $d=2a$, freezing into the $n=3/7$ state occurs at $T\sim0.01V(a)$, and requires about 10 hours of CPU time. We comment on possible freezing scenarios in Sec. X below.

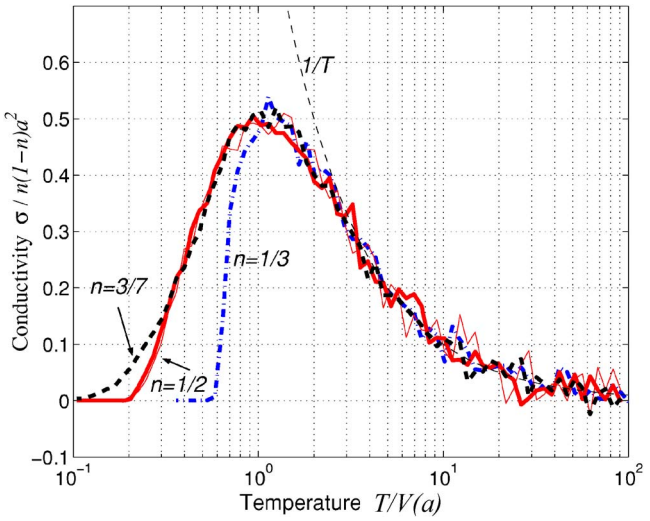

FIG. 4. (Color online) Temperature dependence of the zero bias dc conductivity $\sigma(T)$. Shown are the curves $\sigma/n(1-n)$ for $n=1/3$, $n=1/2$, and for a typical intermediate density (taken here to be $n=3/7$), obtained for the 18×18 system with the screening length $d=2a$. The asymptotic large temperature behavior (21) is indicated by dashed line. The faint solid line, describing $\sigma(T)$ for $n=1/2$ on a 12×12 patch, coincides with that for the 18×18 system, indicating the smallness of finite size effects.

IV. CHARGE TRANSPORT: ELECTRICAL CONDUCTIVITY

Our interest in the hopping transport is twofold. First, the conductivity is experimentally accessible in the dot arrays.[10,11] Second, as we shall see below, the dc conductivity is sensitive to the thermodynamic state, and its temperature and density dependence can thus be used to distinguish between different phases of the system.

Below we use the MC procedure to compute the hopping conductivity in the presence of a small external electric field. The MC conductivity σ_{MC} and the one measured in a real system are related as follows. Electron hopping between neighboring dots is assisted by some energy relaxation mechanism, such as phonons. The latter adds a temperature-dependent prefactor $f(T)$ to the hopping rate, so that $\sigma_{\mathrm{total}}=f(T)\sigma_{\mathrm{MC}}(T)$. [In a simple model involving coupling to acoustic phonons, a golden rule calculation gives a power law $f(T)\propto T^{\alpha}$.] In this work, for simplicity, we shall ignore the system-dependent prefactor $f(T)$, and focus on the MC conductivity σ_{MC}.

The temperature dependence of the MC conductivity, hereafter denoted by σ, is shown in Fig. 4 for several densities. The simulation was performed on a 18×18 patch using the charge-conserving dynamics (type B). The external field $\mathbf{E}$, applied along the patch side, is chosen to be large enough to induce a current measurable in the presence of thermal fluctuations, and yet sufficiently small to ensure the linear response

$$\mathbf{j}=\sigma\mathbf{E}. \tag{15}$$

The data was obtained using E in the range

$$Ea \simeq (10^{-2} - 5 \times 10^{-2})V(a).$$

We observed that the linearity holds for the field values much smaller than both the temperature and the next-to-nearest neighbor interaction, $Ea \ll \min\{V_{nnn}, T\}$ [Eq. (18)].

The conductivity σ, Eq. (15), is obtained using the MC dynamics of type B as follows. Since the field contribution to the potential difference between the adjacent sites separated by $\mathbf{a}=\mathbf{r}_{ij}$, is $-\mathbf{Ea}$, we can incorporate the effect of the field by adding the quantity

$$(q_i - q_j)\mathbf{Ea} \tag{16}$$

to the energy difference $\delta E_{ij}^{(B)}$ in Eq. (8).

Our simulation was carried out using the spin representation, as described in Sec. II C. In the spin language, using the Hamiltonian (11) and the temperature (14), the term corresponding to Eq. (16) is $(s_i - s_j)\mathbf{Ea}$, whereas the system is described by the Hamiltonian (11) with the temperature (14). The data presented below was obtained using the field $\mathbf{E}$ oriented along the height of an elementary lattice triangle, so that $|\mathbf{Ea}| = Ea\cos(\pi/6)$. The spin current density was calculated as

$$j = |\delta s| a \cos\left(\frac{\pi}{6}\right)\frac{\mathcal{N}_+ - \mathcal{N}_-}{\mathcal{N}}, \tag{17}$$

where $\mathcal{N}_\pm$ is the number of hops along (against) the direction of $\mathbf{E}$ during the MC run time, $\mathcal{N}$ is the total number of MC trials at each temperature step, and $\delta s = \pm 2$ is the spin change for each hop. The corresponding charge current is then $j_{\mathrm{el}} = \frac{1}{2}j$.

The MC conductivity as a function of temperature is displayed in Fig. 4 for several values of charge density. From the dependence $\sigma(T)$ one can identify three temperature intervals with different behavior, corresponding to the high, low, and intermediate temperatures. Relevant temperature scales are approximately given by the nearest neighbor and next-to-nearest neighbor interaction strength:

$$V_{nn} = V(a), \quad V_{nnn} = V(\sqrt{3}a). \tag{18}$$

In our MC simulation, for $d=2a$, the value of V_{nnn}, given by the interaction across the main diagonal of a rhombus, was about $0.3V_{nn}$.

The simplest to understand is the high temperature behavior $T \gtrsim V_{nn}$, corresponding to a disordered phase in which conductivity takes place via uncorrelated hops of individual electrons. Conductivity in this phase has a simple temperature and density dependence [see Eq. (21)].

In the opposite limit, at $T \to 0$, the system freezes into the ground state configuration (solid phase), and the conductivity vanishes. The freezing transition is entirely due to the longer range coupling, such as V_{nnn}, since for purely nearest neighbor coupling, realized in the ΔIAFM model, the system does not exhibit a phase transition and is characterized by finite entropy even at $T=0$. Thus the upper temperature scale for the solid phase can be estimated as $T \lesssim V_{nnn}$. The ground state depends on the density n in a complicated way. Near rational n the ground state is commensurate, while at a generic n the state is probably incommensurate. The freezing temperature T_c is also a function of the density n. As the temperature approaches the freezing temperature T_c, the conductivity vanishes (Fig. 4). While the behavior $\sigma(T)$ near $T = T_c$ appears to be singular (see Fig. 4), we were not able to extract the exact form of this singularity directly from our simulation. However, some information about the singularity in conductivity can be obtained from general arguments[15] relating it with the distribution of energies studied in Sec. III. We also observe singularities near rational n in the conductivity dependence on the density, $\sigma(n)$. They are indicated by arrows in Fig. 5.

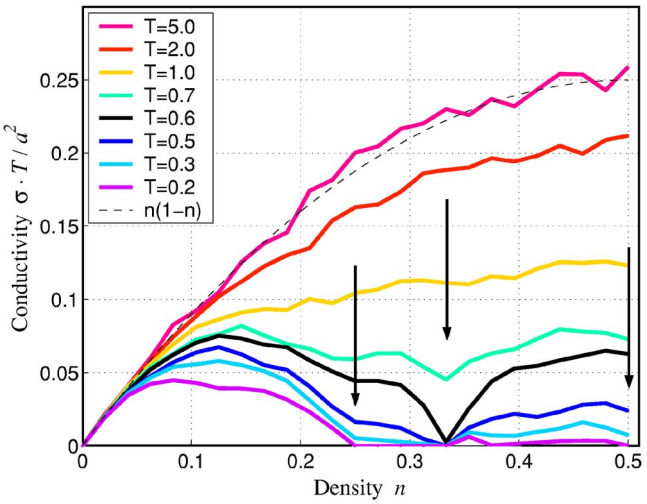

FIG. 5. (Color online) The conductivity σ, scaled by a^2/T, is shown as a function of electron density for several temperatures. The temperature values are given in the units of $V(a)$; the interaction $V(\mathbf{r})$ of the form (2) was used with the screening length $d = 2a$. Arrows mark the features corresponding to the freezing phase transitions at $n = 1/4, 1/3, 1/2$. Dashed line corresponds to the high temperature limit described by Eq. (21).

Finally, at densities $1/3 \lesssim n \lesssim 2/3$ there is an interesting intermediate temperature interval

$$V_{nnn} \lesssim T \lesssim V_{nn} \tag{19}$$

in which the conductivity is finite and reaches maximum as a function of temperature (Fig. 4). Transport at these temperatures is of a collective character (correlated fluid phase) owing to strong short-range correlations between charges which constrain individual charge movements. Due to the frustration, the onset of short-range ordering does not lead to charges freezing. The system appears to possess a sufficient amount of residual entropy to allow for finite conductivity.

An independent consistency check for the MC dynamics is provided by the fluctuation-dissipation theorem,[22] relating current fluctuations to conductivity,

$$\int dt \langle j_\mu(t) j_\nu(0)\rangle = 2\sigma_{\mu\nu}T. \tag{20}$$

Our simulation is found to be in accord with (20) in all temperature regions, which ensures that the MC conductivity indeed describes transport in the linear response regime. [Some deviations from (20) were observed very close to the

freezing point, where σ becomes very small.] In the correlated phase we explicitly evaluate the integral on the left-hand side of (20) by numerically averaging the product $j_\mu(t+\tau)j_\nu(t)$ over τ and t. The result is compared with the conductivity obtained directly from Eqs. (15) and (17) to make sure that during an MC run the system has enough time to reach equilibrium.

At large temperature $T \gg V(a)$, one can evaluate the left-hand side of the fluctuation-dissipation relation (20) explicitly and find the universal high temperature asymptotic behavior of the conductivity,

$$\sigma = a^2 \frac{n(1-n)}{T}. \tag{21}$$

To obtain (21) we note that for a high enough temperature the current is delta-correlated in time,

$$\langle j_\mu(t) j_\nu(0) \rangle = \langle j^2 \rangle \delta_{\mu\nu} \delta(t). \tag{22}$$

The mean square $\langle j^2 \rangle$ can be obtained by summing the probabilities of possible MC moves,

$$\langle j^2 \rangle = \frac{4}{6} \cdot 2n(1-n) \cdot (\delta s)^2 \cdot \left(a \cos \frac{\pi}{6} \right)^2 \cdot w. \tag{23}$$

The factor 4/6 comes about because in the field **E** aligned along the height of the elementary lattice triangle, only four out of possible six bond directions contribute to conductivity. The second factor, $2n(1-n)$, describes the probability to select two adjacent sites occupied by an electron and a hole. The change of occupancy per MC move is $\delta s = \pm 2$, since $s_i = \pm 1$. The expression (23) does not depend on temperature since all the hops are equally probable and uncorrelated, $W_{i\to j} = W_{i\to i} \equiv w = 1/2$ at $T \gg V(a)$. The conductivity tensor is isotropic, $\sigma_{\mu\nu} = \sigma \delta_{\mu\nu}$, as can be explicitly checked by doing a similar high temperature calculation for an arbitrary orientation of the field **E**. Figure 4 shows that the results of our MC dynamics are consistent with the high temperature behavior (21).

The change in conductivity behavior while cooling down from the disordered into the correlated fluid and solid phases can also be seen in Fig. 5. Here we plot the conductivity σ, scaled by a^2/T, as a function of the electron density n for several temperatures. The results, shown for the densities $0 \leqslant n \leqslant 1/2$, can be extended to $n > 1/2$ using the electron-hole symmetry $n \leftrightarrow 1-n$. The high temperature curve is clearly consistent with the $n(1-n)$ dependence (21). The low temperature curves indicate that the conductivity vanishes more quickly near the densities of a simple fraction form $(n = 1/4, 1/3, 1/2)$. This corresponds to freezing of the system into a commensurate state at these values of n. The commensurate states at $n = 1/3$ and $n = 1/2$ are shown in Fig. 6 [panels (a) and (c), respectively].

At densities near these simple fractional values, the system conducts via hops of excess electrons or holes moving in the frozen crystalline background. Such a situation is depicted in Fig. 6 [panel (b)] for the case of $n = 1/3 + \epsilon$. Since the conductivity is proportional to the excess charge density ϵ, we expect $\sigma(n)$ to have cusps near simple fractional densities. Such cusps are indeed seen in Fig. 5 near $n = 1/4, 1/3, 1/2$.

V. THE HEIGHT VARIABLE

A. The ground state

Here we attempt to understand the ordering in the ground state and in the correlated fluid by employing the notion of the height field-order parameter, originally introduced in the context of the ΔIAFM problem by Blöte *et al.*[17,18] In our model (1) and (2), the latter problem corresponds to the limit $d \ll a$ dominated by the nearest neighbor interactions. The essential features of the ground state can be understood by considering energy minimization for individual plaquettes (triangles). With only two kinds of charges it is impossible to avoid the frustrated bonds between the like charges, with at least one such bond per triangle. In the ground state, the number of such bonds must be as small as possible. That can be achieved by pairing the neighboring triangles in such a way that each pair shares a frustrated bond. One can see that the charge state corresponding to all triangles paired, while providing the absolute energy minimum, is not unique. On the contrary, the pairing condition leaves plenty of freedom in the charge configuration, characterized by extensive entropy (finite entropy-to-area ratio).

The configurations permissible by the pairing condition have a simple geometric interpetation. After erasing all frustrated bonds, one obtains a rhombic tiling of the triangular lattice,[17,18] as shown in Fig. 6 [panels (a)–(e)]. It is convenient to view such a tiling as a 2D surface in a 3D cubic crystal projected along the (111) axis on a perpendicular plane. After undoing the projection by lifting the 2D configuration of rhombi in the 3D space, each site $\mathbf{r}_i$ acquires a scalar variable $h(\mathbf{r}_i)$ which is the height of the lifted surface in a 3D cubic crystal. The field h takes values which are multiples of the distance between the cubic crystal planes,

$$b = \frac{\ell}{3} = \frac{a}{\sqrt{2}}, \tag{24}$$

where ℓ is the main diagonal of the unit cell in the cubic crystal. The mapping onto a continuous height surface exists only for the densities $1/3 \leqslant n \leqslant 2/3$, which we focus on hereafter, since for n outside this interval the tiling contains voids.

As we discussed above, the long range character of the interaction (2) lifts the ground state degeneracy, leading to freezing into specific ground states. To use the height variable to characterize the ordering, we define the slope **t** of the height surface. For that we consider the surface normal vector

$$\mathbf{m} = \mathcal{A}^{-1} \sum_{s=1}^{3} r_s \mathbf{e}_s, \quad \mathcal{A} = r_1 + r_2 + r_3 \tag{25}$$

where r_1, r_2, r_3 are the numbers of rhombi formed by $(\mathbf{e}_2, \mathbf{e}_3)$, $(\mathbf{e}_3, \mathbf{e}_1)$, $(\mathbf{e}_1, \mathbf{e}_2)$ which add up to the total area $\mathcal{A} = N^2$.

The slope **t** is given by the projection

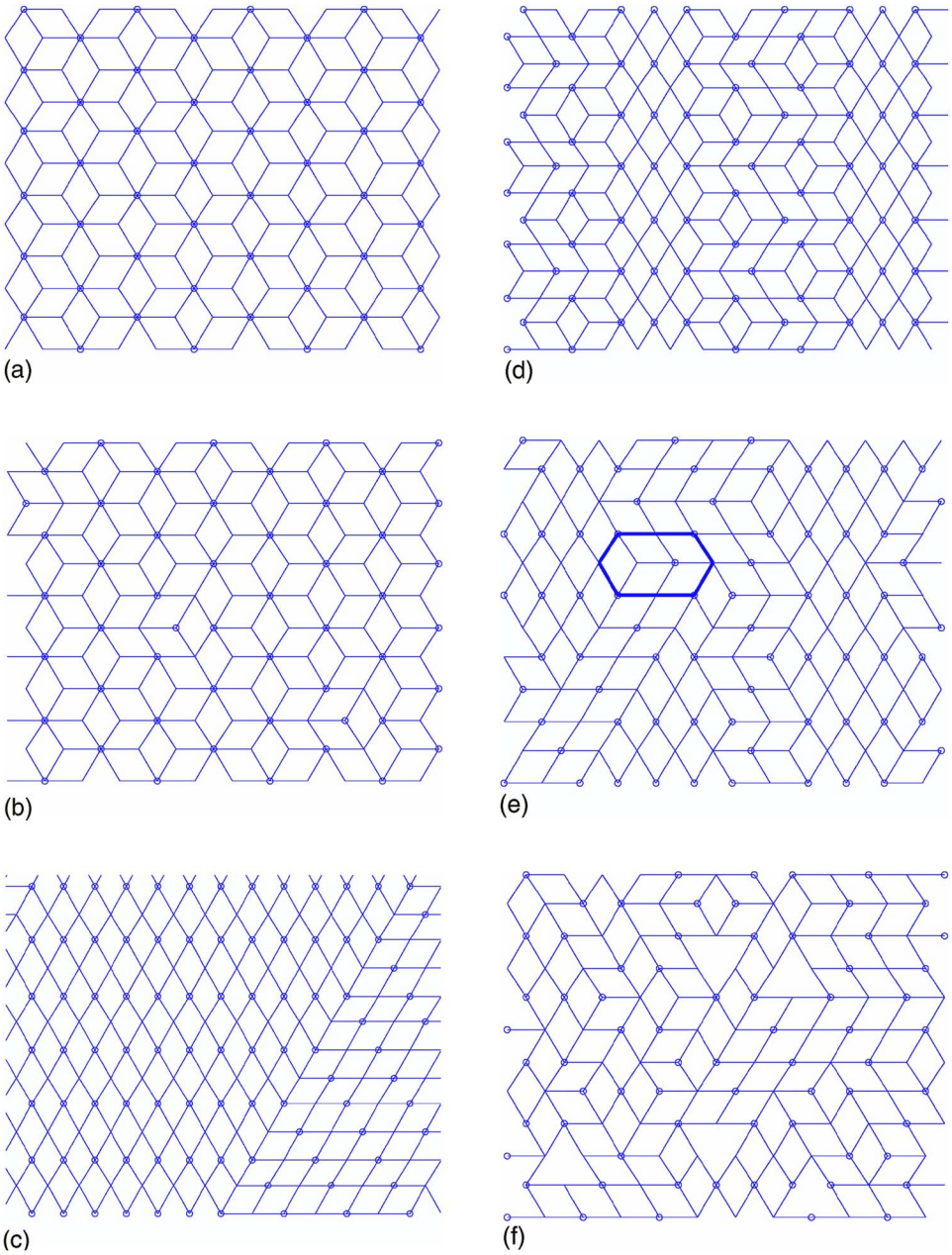

FIG. 6. (Color online) (a) Commensurate $\sqrt{3}\times\sqrt{3}$ charge ground state at the density $n=1/3$. Electrons are represented by small dots on the triangular array sites. Pairing of the triangles is revealed by erasing all frustrated bonds connecting the sites with equal occupancy, as described in Sec. V. (b) Typical charge configuration for $n=1/3+\epsilon$. There are three excess charges in the system ($\epsilon=3/144$) hopping over the honeycomb network of unoccupied sites in the state shown in panel (a). The excess carriers, dilute at $\epsilon\ll 1$, are moving nearly independently on the frozen $\sqrt{3}\times\sqrt{3}$ state background. (c) Ground state for $n=1/2$. Shown are the two charge density wave domains characterized by different slope orientations [Eq. (26)]. (d) Example of a ground state for a commensurate density with a higher denominator, here $n=3/7$. (e) Typical charge configuration obtained in a simulation for $n=1/2$ in the correlated fluid phase. Two elementary 3D cubic cells corresponding to a free charge are marked. (f) Typical charge configuration for $n=1/2$ at temperature somewhat higher than in panel (c). In this case, there are several topological defects (unpaired triangles) present in the system. These defects can be interpreted as dislocations of the height field (see Sec. V).

$$\mathbf{t}=\mathbf{m}-(\hat{\mathbf{z}}\cdot\mathbf{m})\hat{\mathbf{z}},\quad \hat{\mathbf{z}}=\frac{1}{\sqrt{3}}(\mathbf{e}_1+\mathbf{e}_2+\mathbf{e}_3). \tag{26}$$

Here the vectors $\mathbf{e}_s$, $s=1,2,3$ form the basis of the auxiliary 3D crystal (Fig. 10 in the Appendix), and r_s give the numbers of 3D crystal faces normal to the vectors $\mathbf{e}_s$. Equation (26) defines an average slope of the configuration. For a smooth surface, the vector $\mathbf{t}(\mathbf{r})$ is proportional to the local height gradient, $\mathbf{t}(\mathbf{r})\propto(\partial_x h,\partial_y h)$.

When the interactions are of the nearest neighbor kind ($d\ll a$), the height surface fluctuates freely even at small T. We observe a similar behavior at finite temperatures (above freezing) for the system with the long-range interaction (2). The numbers r_s, $s=1,2,3$, for an $N\times N$ patch are equal on average, fluctuating around the mean value of $N^2/3$, and thus the average slope is $\mathbf{t}=\mathbf{0}$. As $T\to 0$, for the studied densities $n=1/3,2/3$, and $n=1/2$, the interaction (2) leads to freezing into commensurate ground states characterized by specific discrete slopes and a nonextensive entropy.

B. The correlated fluid

The height field h is defined globally and uniquely (modulo an additive constant and an overall sign) for any of the degenerate ground states of the ΔIAFM model. For $T>0$, however, due to thermal fluctuations, some of the triangles are left unpaired. Such unpaired triangles represent topological defects of the height field. This can be seen most clearly at low T, when the defects are dilute, and the height field can be constructed locally around each defect. It then turns out that the height field, considered on a closed loop surrounding a defect, is not a single-valued function.[29]

The topological charge assignment in this situation is facilitated by interpreting the defects as screw dislocations, centered at the unpaired triangles. Positions of the dislocations are seen as large (2×2) triangles in Fig. 6(f). After integrating ∇h over a contour enclosing a single triangle, one obtains a positive or negative mismatch in the height h equal to the dislocation Burgers vector

$$b_\Delta = \oint \partial_i h dx_i = \pm 2\ell = \pm 6b. \tag{27}$$

The topological charge algebra is indeed identical to that of dislocations (Z). Following a loop around two dislocations of opposite sign (27), gives net zero charge, $\oint \partial_i h dx_i = 0$. The topological nature of the defects constrains the dynamics. During the MC simulation, the dislocations originate and disappear only in pairs.

The minimal energy cost required to create a defect can be estimated as the energy for unparing of two triangles. Each unpaired triangle adds one more frustrated bond which can be shared by neighboring triangles [see Fig. 6(f)]. The corresponding energy cost is $2V(a)$ per unpaired triangle. At sufficiently low temperatures the probability of creating a pair of defects is therefore exponentially suppressed, $P \sim e^{-4V(a)/T}$. On the other hand, at a high temperature $T \gg V(a)$ the defects are so abundant that the height field ceases to exist even as a local notion. In this high temperature state, marked disordered phase in Fig. 3, electron hopping is uncorrelated, with the interaction enforcing single or zero occupancy, and otherwise playing no role.

At lower temperatures, $T \lesssim V(a)$, with the fugacity of a single defect decreasing at least as $e^{-2V(a)/T}$, the defects quickly become dilute. In this case, the height field is defined locally in the entire plane, except the vicinity of the defects. The collective behavior of defects in the correlated phase, such as the Kosterlitz-Thouless unbinding transition, is controlled by entropic effects which will be analyzed below in Sec. VII.

The charge rearrangements that do not produce or destroy defects cost no energy in the ΔIAFM model limit $d \ll a$. In the case of a long-range interaction, such rearrangements generally cost finite energy which is determined by the V_{nnn} interaction strength. An example of a typical single electron move that preserves the structure of rhombic tiling is shown in Fig. 7. We find that the state with a height field, despite being constrained by the triangle pairing condition, allows for sufficiently large number of movable charges which can lead to macroscopic charge rearrangements which do not produce defect pairs. The MC conductivity appears to be related to these rearrangements, hereafter referred to as *free charges*. As Fig. 7 illustrates, the moves associated with free charges can be interpreted geometrically as changing the 3D lifted tiling by adding or removing two adjacent cubes. This operation does not introduce defects or discontinuities in the lifted surface, preserving its 3D continuity.

In our MC study, with electron densities $1/3 \lesssim n \lesssim 2/3$, we found that there is a temperature interval in which the number of topological defects (unpaired triangles) is small, and thus the height order parameter is well defined. Simultaneously, the density n_f of the free charges (see Fig. 7) was observed to be large. During MC simulations we accumulate a histogram for n_f and find that this is a nonconserved quantity with a broad Gaussian distribution. The mean $\overline{n_f}$ is of the order of 10%–50% of the total electron density n for the temperatures

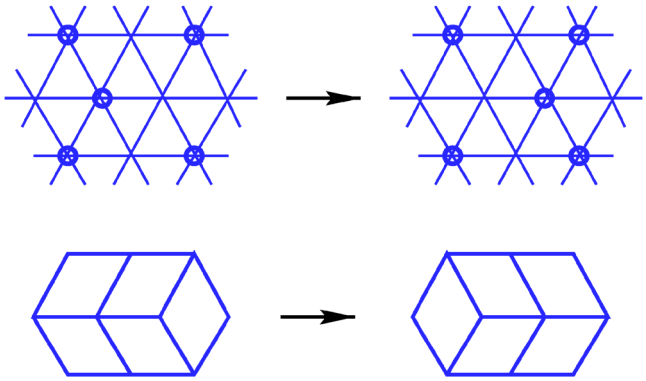

FIG. 7. (Color online) The concept of free charges in the correlated phase, which can move without changing the number of frustrated bonds, is illustrated. Above, an example of a free charge move; below, the corresponding change in the rhombic tiling.

$$V_{nnn} \lesssim T \lesssim V_{nn} \tag{28}$$

between the nearest neighbor interaction V_{nn} which enforces pairing correlations, and the next-nearest interaction V_{nnn} which controls freezing at low temperature.

The correlated nature of the charge state at these temperatures, owing to the continuous height variable constraint, leads to a peculiar picture of charge flow. The notion of individual electron hopping must be replaced by a more adequate picture involving fluctuations of the height field giving rise to charge movement. We observe that the Ohmic conductivity remains finite (Fig. 4) in the correlated fluid temperature interval, while the topological defects freeze out. It appears that the height fluctuations on their own are sufficient for charge transport and conductivity. The elementary height fluctuations, embodied in the notion of free charges (Fig. 7), represent MC moves of an effective nonconserving (type A) dynamics of the 2D surface. Based on this idea, in Sec. VIII we shall develop a continual approach to describe the dynamics in the correlated state.

One may expect that the free charges, although nominally allowed to only move back and forth (Fig. 7), can propagate over the whole system. Microscopically this happens since a move of one free charge unlocks subsequent moves of other free charges. This picture is consistent with our observations based on MC dynamics: In Sec. VI we find a non-vanishing contribution to the conductivity in the absence of dislocations. The dislocationless conductivity points to the importance of free charges in transport. However, more work will be needed to address other properties of free charges dynamics, such as the microscopic transport mechanism and ergodicity.

To assess the relevance of this conductivity mechanism for real systems one needs to understand several issues, the

most important one being the role of disorder. Although our MC study of the disordered problem was not too extensive and, in particular, restricted to not too low temperatures, it allows to draw some assuring conclusions. In general, for weak disorder we observe no change in the qualitative features of the dynamics. We studied the dc conductivity in presence of a finite amount of disorder, modeled by the random potential $\phi(\mathbf{r}_i)$ in the Hamiltonian (11). The MC simulation used statistically uncorrelated random $\phi(\mathbf{r}_i)$ with a uniform distribution in the interval $-\phi_0 \leq \phi(\mathbf{r}_i) \leq \phi_0$, where $\phi_0 \sim V_{nnn} = V(\sqrt{3}a)$. The only significant difference observed was a relatively more slow time averaging in the presence of disorder, leading to enhanced fluctuations of the conductivity recorded as a function of temperature. Otherwise, the qualitative behavior of the conductivity was found to be the same as in the clean system. In particular, the zero bias conductivity remains finite in the correlated fluid phase in the presence of disorder. We attribute the robustness of conductivity against weak disorder to the nonconserving dynamics of the height variable, which is not pinned by the disorder in the temperature interval of interest.

VI. DISLOCATION-MEDIATED VERSUS HEIGHT FIELD-MEDIATED CONDUCTIVITY

Here we investigate in detail the effect of dislocations on electron transport in the correlated phase. As noted above, certain charge moves, associated with "free charges" (Fig. 7) have relatively low energy cost. These moves correspond to height field fluctuations which do not produce topological defects. The presence of the pairing correlations described by the height variable and the dynamics of free charges associated with these correlations, poses an interesting question regarding the relative contribution of the free charges and dislocations to the transport.

One approach to understand the role of dislocations would be to forbid entirely the charge hops that introduce new dislocation pairs and study MC conductivity in such a system. We have tried to modify the MC simulation in this way, and found that the dislocationless system exhibits finite conductivity solely due to free charges, indicating that the dislocations are not essential for conductivity. This method, however, does not allow to compare the role of dislocations and free charges quantitatively, since the rule introduced to eliminate dislocations alters the dynamics in an uncontrollable way. In fact, since the definition of conductivity changes in the dislocationless MC, although we indeed observe a nonzero conductivity, it is difficult to compare the resultant "dislocationless" conductivity with that of the original problem. Instead, we adopt a different, more gentle approach. We employ the same dynamics as above (conserving, or type *B*), in which we detect dislocations and analyze *partial conductivities* σ_p in the presence of $p=0,1,2,\ldots$ dislocation pairs (Fig. 8).

Let us outline the corresponding MC procedure. We introduce a small bias $\mathbf{E}$ across the finite system with periodic boundary conditions, and define the partial conductivities σ_p similarly to the total conductivity calculated as described in Sec. IV, Eq. (15),

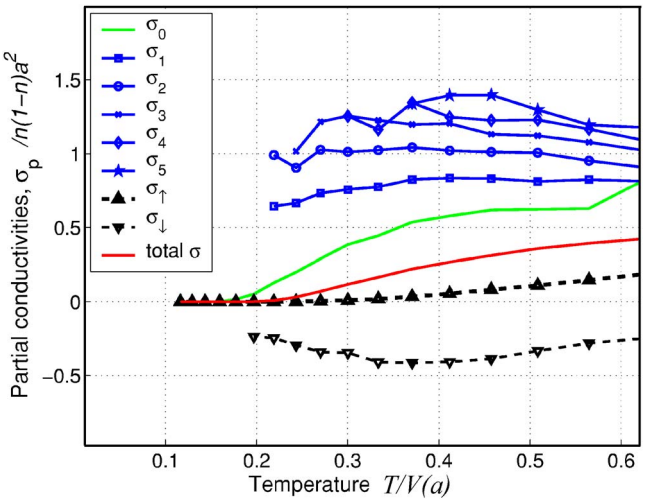

FIG. 8. (Color online) Partial conductivities σ_p, $p=0,\ldots,5$, which account for MC moves in the presence of p dislocation pairs (see text), for the 12×12 patch, density $n=\frac{1}{2}$, screening length $d=2a$, Eq. (2). The dislocationless conductivity σ_0 approaches zero continuously at the freezing transition, while the conductivities σ_p, $p\neq0$ remain finite. Separately shown are the conductivities $\sigma_\uparrow$ and $\sigma_\downarrow$ that correspond to the MC steps changing the number of dislocation pairs. (Note the negative sign $\sigma_\downarrow<0$.)

$$\mathbf{j}_p = \sigma_p \mathbf{E}. \tag{29}$$

The partial currents j_p at a fixed number p of the dislocation pairs are defined similarly to the total current, Eq. (17), with the numbers of hops $\mathcal{N}_\pm$, $\mathcal{N}=\mathcal{N}_+ + \mathcal{N}_-$, replaced by the p-dependent $\mathcal{N}_{p_\pm}$ and $\mathcal{N}_p = \mathcal{N}_{p_+} + \mathcal{N}_{p_-}$. Here $\mathcal{N}_p$ is the total number of MC trials, or attempted hops that may or may not lead to real hops, in which a pair of randomly selected neighboring sites is such that the charge hop between them would preserve the number p of dislocation pairs. Accordingly, $\mathcal{N}_{p_+}$ and $\mathcal{N}_{p_-}$ descibe charge hop trials along and opposite to the applied field with a fixed number p of dislocations. The actual hop is then attempted with a Boltzmann probability (7), as discussed in Sec. II. In our simulation we studied the system 12×12 at density $n=\frac{1}{2}$.

The partial conductivities σ_p, $p=0,1,2,\ldots$, describing the contribution to transport of charges hopping in the presence of the $2p$ dislocations, need to be complemented by two additional parts, $\sigma_\uparrow$ and $\sigma_\downarrow$, describing the conduction processes which alter the number of dislocations. Indeed, a significant fraction of the occupied-empty site pairs chosen in the MC simulation are such that upon a charge hop between them the dislocation number would either increase or decrease. Such hops, if selected by the Boltzmann probabilities, can also carry current in the presence of the applied bias (as illustrated in Fig. 8). With the corresponding numbers of the MC trials denoted by $\mathcal{N}_\uparrow$ and $\mathcal{N}_\downarrow$, the total number of attempts is

$$\mathcal{N} = \mathcal{N}_0 + \mathcal{N}_1 + \mathcal{N}_2 + \cdots + \mathcal{N}_\uparrow + \mathcal{N}_\downarrow. \tag{30}$$

The partial MC attempt numbers $\mathcal{N}_p$, $\mathcal{N}_\uparrow$, $\mathcal{N}_\downarrow$ temperature dependence is summarized in Fig. 9.

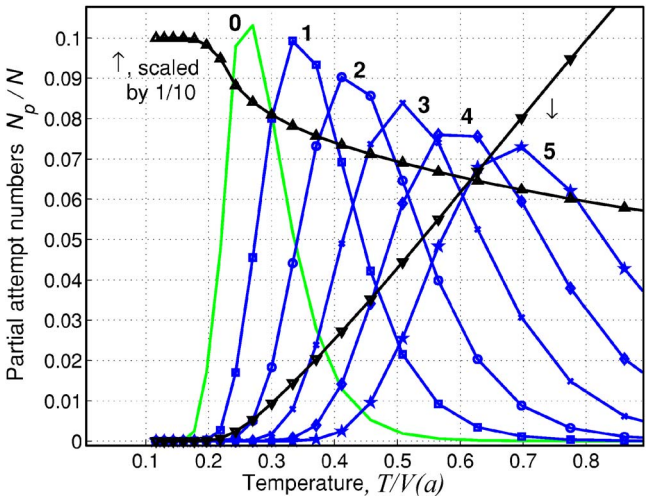

FIG. 9. (Color online) Partial attempt numbers scaled by $\mathcal{N}$ define normalized weights $\mathcal{N}_p/\mathcal{N}$, $p=0,\ldots,5,\uparrow,\downarrow$, for the partial conductivities σ_p of Fig. 8. The total $\mathcal{N}$ [Eq. (30)] was approximately constant, varying by less than 5% in the whole temperature range. With the $\mathcal{N}\approx 3\cdot 10^8$ per temperature step, the whole simulation took about 15 hours on a 1.25 GHz PowerPC.

As Figs. 8 and 9 illustrate, the average number of dislocations in the 12×12 patch evolves from about 5 at $T\approx 0.7V(a)$ to zero in the vicinity of the freezing transition. As the temperature lowers, most of the time the system attempts to create dislocation pairs ($\mathcal{N}$ is dominated by $\mathcal{N}_\uparrow$), however, almost all of these attempts are discarded due to their exponentially low Boltzmann weight, resulting in the negligible current $j_\uparrow$ and partial conductivity $\sigma_\uparrow$ (see Fig. 8).

We note a drastic difference between the dislocationless conductivity σ_0 and the partial conductivities $\sigma_{p\neq 0}$ near the freezing transition at $T_c\approx 0.2V(a)$. Whereas the former approaches zero continuously as $T\to T_c$, the latter have an apparent steplike discontinuity. However, the contributions of partial conductivities σ_p, $p\neq 0$, to the total conductivity

$$\sigma=\mathcal{N}^{-1}\sum_{p=0,1,2,\ldots,\uparrow,\downarrow}\mathcal{N}_p\sigma_p \tag{31}$$

are small, since the weights $\mathcal{N}_{p\neq 0}/\mathcal{N}$ drop very quickly as T approaches T_c (Fig. 9). In a relatively small 12×12 system studied here, the dislocations are almost always totally absent near T_c. In this case the total conductivity (31) is dominated by σ_0 (Fig. 8), due to small $\mathcal{N}_{p\neq 0}/\mathcal{N}$. This is consistent with the observation that the total conductivity decreases to zero in a continuous fashion near T_c, similar to σ_0, with the steplike contribution of $\sigma_{p\neq 0}$ being inessential.

One cannot exclude, however, a different regime in a large system, where the discontinuous part $\sigma_{p\neq 0}$ of the total conductivity (31) can become dominant in the thermodynamic limit, due to dislocation number growing with system size. Even in this case, we expect the dislocationless contribution to the conductivity to remain significant. In that regard, we note an approximately constant increment in conductivity $\Delta_p\sigma=\sigma_{p+1}-\sigma_p\approx$const when the number of dislocations increases by one, $p\to p+1$, observed at temperatures not too close to freezing (Fig. 8). The approximately p-independent $\Delta_p\sigma$ provides an estimate of the conductivity per dislocation, suggesting that in the dilute regime the dislocations contribute to transport approximately independently. However, the dislocationless part σ_0 is a few times larger than $\Delta_p\sigma$, providing a constant offset to the σ_p vs p dependence. It is thus not inconceivable that, if the dislocations are suppressed, e.g. due to Kosterlitz-Thouless transition, or otherwise, the conductivity would remain finite, dominated by the dislocationless contribution.

This conclusion is reinforced by the results of MC simulation with the rules modified so that the dislocations are totally excluded, as discussed above. In this case, we find finite conductvity, behaving as a function of temperture at $T>T_c$ in a way similar to σ_0. Interestingly, the freezing transition is unaffected by this alteration, with the same value of T_c observed under changed MC rules. These observations, in our view, leave no doubt that the conductivity does not entirely depend on dislocations. The transport of free charges, responsible for the dislocationless contribution σ_0, gives rise to finite conductivity independent of dislocations.

Interestingly, the partial conductivity due to annihilation of the topological defect pairs is negative, $\sigma_\downarrow<0$. While we do not have a complete understanding of this observation, we mention one possible explanation which involves a nonlinear effect. We suppose that a large enough electric field can perturb the system so that its relaxation back to equilibrium will be accompanied by release of a charge in the opposite direction. However, our MC study indicates that the relative weight of such processes, and thus its contribution to the conductivity, is small near the freezing transition (Fig. 9). Therefore, in our view, the associated nonlinear conductivity is not essential for the interpretation of the numerical data.

The described analysis of partial conductivities does not reveal the microscopic mechanism by which dislocations facilitate transport. One possibility is that the conduction is due to the motion of dislocations themselves (since they are charged objects). Another possibility is that the mere presence of dislocations facilitates the hops of free charges in their vicinity and results in a finite conductivity. While our MC study does not provide a definite answer, it is possible that the two alternatives are not unrelated, since the motion of a dislocation can happen due to a free charge movement right next to it.

To summarize, we have shown that the dislocation pairs facilitate conductivity, and have compared their contribution with dislocationless conductivity due to free charges. While in the model analyzed here there is no obvious way to completely separate these contributions, due to the absence of a dislocation binding transition, we conclude that both contributions are present, with their relative importance depending on the dislocation density.

VII. FLUCTUATIONS IN THE CORRELATED PHASE: DISLOCATIONS UNBINDING

The height field describes the effect of frustration on charge dynamics by providing a nonlocal change of variables that helps to keep track of the local correlations between charges. However, as we found above, in general the height

variable cannot be globally defined due to the presence of dislocations. Nonetheless, at relatively low temperature, when dislocations are dilute, the height field provides a useful description on a local level.

Here we adopt the view that the dynamics of the height field is simpler than the underlying charge dynamics. Indeed, while the latter is strongly constrained, the fluctuations of the height field appear to be Gaussian. The height variable also provides a natural continual description employed to study dislocation unbinding (this section), roughening transition (Sec. VIII), the dynamics (Sec. IX) as well as the freezing into commensurate states (Sec. III B above).

The MC dynamics in the correlated state can be interpreted as the height field fluctuations. These fluctuations dominate in the temperature interval (28) where the dislocations are dilute. Thus here we consider the height field ignoring for some time the effect of dislocations. We study the height fluctuations numerically and find that in the continuum limit $r \gg a$ they are described by the partition function of the form

$$Z_0 = \int \mathcal{D}h(\mathbf{r}) e^{-\int d^2\mathbf{r}(\kappa/2)(\nabla h)^2}, \tag{32}$$

where κ is an effective stiffness of the height surface, with temperature incorporated into κ.

The Gaussian partition function (32) has been introduced by Blöte and Hilhorst,[17] and by Niehnuis *et al.*[18] for the height field in the ΔIAFM model at $T \to 0$. The corresponding stiffness has been obtained from the exact solution[16,18]

$$\kappa_{\Delta\mathrm{IAFM}} = \frac{\pi}{9b^2}. \tag{33}$$

[Note that, instead of the stiffness κ, Ref. 18 employs the "renormalized temperature" $T_R = 2\pi/\kappa b^2$, with $T_R = 18$ for the ΔIAFM.] The equilibrium height fluctuations have been studied numerically[30,31] in the case of the nearest neighbor interactions, confirming the result (33) for the ΔIAFM.

Here we extend these results to the model with long-range interaction. We study the fluctuations of the height field numerically, by assigning the heights $h(\mathbf{r}_i)$ to the triangular lattice sites $\mathbf{r}_i$ according to the procedure described in the Appendix. The results of this study can be summarized as follows.

(i) At fixed temperature, we accumulate the histograms $\mathcal{P}[h(\mathbf{r}_i)]$ of height values for a set of points $\{\mathbf{r}_i\}$ in the $N \times N$ patch. We find that the fluctuations are Gaussian,

$$\ln \mathcal{P}[h(\mathbf{r}_i)] \propto -h^2(\mathbf{r}_i), \tag{34}$$

independently for each point $\mathbf{r}_i$. This suggests that a partition function of the form (32) can be employed.

(ii) To calculate the effective stiffness for a system with the long-ranged interaction (2), we fit the two-point height correlator to the one following from Eq. (32):

$$\langle (h(\mathbf{r}_i) - h(\mathbf{r}_j))^2 \rangle = \frac{1}{\pi\kappa} \ln \frac{|\mathbf{r}_{ij}|}{r_0}, \tag{35}$$

with the length r_0 of the order of the lattice constant a. For this analysis we generate random MC configurations, selecting the height surfaces of zero average slope, defined as in Eq. (26) above.

We tested this procedure by calculating the stiffness in the nearest neighbor interaction limit $d \ll a$ at $n = 1/2$. The MC dynamics recovers the value $\kappa_{\Delta\mathrm{IAFM}}$, Eq. (33), within a few percent accuracy. With the long-range interaction, the relationship (35) still holds, allowing us to determine κ. We systematically find the values of κ below $\kappa_{\Delta\mathrm{IAFM}}$, Eq. (33).

(iii) The measured stiffness κ can be used to assess the possibility of a dislocation-binding transition of the Kosterlitz-Thouless kind.[32,33] If exist, such a transition between the disordered and correlated fluid phases would realize[34,35] the KTHNY 2D melting scenario. Dislocation binding takes place above the universal threshold value

$$\kappa > \kappa_{\mathrm{KT}} = \frac{8\pi}{b_\Delta^2}, \tag{36}$$

with b_Δ the Burgers vector of the dislocation. Using the value from Eq. (27), one obtains $\kappa_{\mathrm{KT}} = 2\kappa_{\Delta\mathrm{IAFM}}$. Thus the KT transition is absent in the zero-field ΔIAFM.[18]

We find that this conclusion remains valid for the long-range interaction. For the interaction (2), the stiffness decreases as a function of d. For typical d used in this work, stiffness values are a few times smaller than $\kappa_{\Delta\mathrm{IAFM}}$. Although such a behavior may seem counterintuitive (one could expect the system to become stiffer for an interaction of longer range), it is in fact consistent with the scaling arguments presented in Sec. VIII B. It is also compatible with the observation[18] that the ferromagnetic second-neighbor coupling causes increase of stiffness. In agreement with this, adding longer-range antiferromagnetic couplings should lead to the decrease of κ.

We conclude that the dislocations are always unbound in our system. This is indicated by a crossover (rather than a sharp transition) between the disordered and correlated phases in the phase diagram, Fig. 3. Thus, in the thermodynamic limit, the dislocation pairs are present at any temperature. While their concentration may be small, it is nonzero, and, strictly speaking, the height field is not well defined in an infinite system. However, in a finite system we often observe that dislocations are absent at low temperature, which justifies the height field as a local notion.

VIII. THE ROLE OF HEIGHT FLUCTUATIONS NEAR FREEZING TRANSITION

Although the height surface fluctuates freely in the correlated phase, the stiffness values κ obtained from the MC dynamics are found to be below the bound[18] necessary for the fluctuation-induced roughening transition.[36] In this respect, the case of the long-range interaction (2) appears to be qualitatively similar to that of the ΔIAFM in the small field.[18,34] The purpose of the present section is to rationalize this similarity, and quantify the reduction of stiffness (as compared to that of the ΔIAFM) by employing renormalization group methods.

Below we construct the free energy for the charge denstity and the height field, with a coupling of a sine-Gordon form,

and present its scaling analysis. We obtain a bound on the effective stiffness κ, Eq. (54), and, by comparing it to that found from the MC dynamics, determine that the continuous roughening transition does not take place. Rather, as discussed in Sec. III, freezing occurs via a finite-order transition. The bound (54) indicates that the height fluctuations are irrelevant, and, as a result, allows us to rule out both instances of the continuous transitions (dislocation-unbinding, and roughening). Subsequently, in Sec. IX, we use the developed formalism to study equilibrium current fluctuations and conductivity.

A. Free energy

The correlated state is described in terms of the height variable $h(\mathbf{r})$ and charge density $n(\mathbf{r})$. Microscopically the state of the system is defined uniquely by specifying either the former or the latter. However, here we demonstrate by scaling analysis that at large length scales the height and density fluctuations decouple. This obeservation allows us to employ a partition function with h and n as independent variables,

$$Z_{\rm corr} = \int \mathcal{D}h(\mathbf{r})\mathcal{D}n(\mathbf{r}) e^{-\mathcal{F}[h,n]}. \tag{37}$$

Here the free energy

$$\mathcal{F}[h,n] = \mathcal{F}_h + \mathcal{F}_n + \mathcal{F}_{\rm int} \tag{38}$$

is a sum of the contributions of the height field, the charge density, and their interaction. As before, the temperature is incorporated into $\mathcal{F}$.

The phenomenological free energy $\mathcal{F}_h$ has the form

$$\mathcal{F}_h = \int d^2\mathbf{r}\left(\frac{\kappa}{2}(\nabla_{\mathbf{r}} h)^2 + g\cos\frac{2\pi h}{b} + f\cos\frac{\pi h}{b}\right), \tag{39}$$

with κ the stiffness. Here the term $\cos(2\pi h/b)$ assigns higher statistical weight to the field configurations that pass through the points of the 3D cubic lattice, with the period b in height given by Eq. (24). The third term in (39) describes the coupling of charge to the chemical potential, in our case realized as the gate voltage,

$$f = C\bar{n}eV_g, \tag{40}$$

with $\bar{n}$ the average charge density and $C \simeq T^{-1}$. The coupling of the form $\cos(\pi h/b)$, with the period $2b$ in height, arises because opposite charges occupy two different sublattices of the 3D lattice, alternating in the height direction.[18] The third term in Eq. (39) is always more relevant than the second one in the sense of scaling.

Consider now the charge density $n_{\mathbf{r}}$. Electrons interact with each other and with an external electrostatic potential $\Phi^{\rm ext}(\mathbf{r})$, which gives

$$\mathcal{F}_n = \frac{1}{2}\int d^2\mathbf{r}d^2\mathbf{r}' n_{\mathbf{r}} U_{\mathbf{r}-\mathbf{r}'} n_{\mathbf{r}'} + \int d^2\mathbf{r} n_{\mathbf{r}}\Phi^{\rm ext}(\mathbf{r}) \tag{41}$$

with the interaction $U_{\mathbf{r}-\mathbf{r}'}$ of the form (2).

The coupling between the density and the height variable should be periodic in $2b$ for the same reason as in Eqs. (39) and (40), with $\bar{n}$ replaced by the fluctuating density,

$$\mathcal{F}_{\rm int} = \lambda\int d^2\mathbf{r} n_{\mathbf{r}} \cos\frac{\pi h_{\mathbf{r}}}{b}. \tag{42}$$

Scaling analysis of the problem (38) is presented below.

B. Scaling analysis

The nonlinear terms in Eqs. (39) and (42) acquire nontrivial scaling dimensions due to fluctuations. At one loop, the anomalous dimensions of the couplings f, λ, and g are

$$X_f = X_\lambda = \frac{2\kappa^*}{\kappa}, \tag{43}$$

$$X_g = \frac{8\kappa^*}{\kappa}, \tag{44}$$

where we define

$$\kappa^* \equiv \frac{\pi}{8b^2}. \tag{45}$$

The term $f\cos(\pi h/b)$ becomes relevant when $X_f < 2$, or

$$\kappa > \kappa_f = \kappa^*. \tag{46}$$

The coupling g becomes relevant at a larger stiffness,

$$\kappa > \kappa_g = 4\kappa^*. \tag{47}$$

The coupling λ between the density and height fields is relevant when the scaling dimension of the gradient term is larger than the sum of scaling dimensions of λ and n. The field n is not renormalized since its free energy is quadratic. From (41), the bare dimension of n is $X_n = 3/2$. Hence the height-density interaction is relevant when

$$X_\lambda + X_n < 2, \quad \text{or } \kappa > \kappa_\lambda = 4\kappa^*. \tag{48}$$

The nonlinear terms in (39) do not renormalize the stiffness κ at one loop. However, the stiffness may obtain a one loop correction $\delta\kappa$ due to the interaction with the density, Eq. (42). Below we consider such a possibility.

Since the free energy $\mathcal{F}_n$ is Gaussian, we integrate out the field $n_{\mathbf{r}}$ in (37) and obtain an effective free energy for the height field,

$$\tilde{\mathcal{F}}_h = \mathcal{F}_h - \frac{\lambda^2}{2}\sum_{\mathbf{k}}\left(\cos\frac{\pi h}{b}\right)_{-\mathbf{k}}\frac{1}{U_{\mathbf{k}}}\left(\cos\frac{\pi h}{b}\right)_{\mathbf{k}}. \tag{49}$$

Consider the case of the screened Coulomb interaction of the form (2),

$$U_{\mathbf{k}} = \frac{2\pi}{k}(1 - e^{-kd}). \tag{50}$$

At length scales larger than the screening length, $kd \ll 1$,

$$\frac{1}{U_{\mathbf{k}}} \approx \frac{1}{2\pi}(A + Bk) \tag{51}$$

with $A = 1/d$, $B = 1/2$. For the unscreened interaction, $(U_{\mathbf{k}})^{-1}$ is of the form identical to (51) with $A = 0$, $B = 1$. The local

term $A/2\pi$ corrects the coupling constant g and does not contribute to the stiffness. The correction to stiffness $\delta\kappa$ arises from the nonlocal part of (49) with $U_{\mathbf{k}}^{-1} \to Bk/2\pi$. Expanding $\cos \pi h/b = (e^{i\pi h/b} + e^{-i\pi h/b})/2$, we note that the terms $(e^{i\pi h/b})_{-\mathbf{k}}(e^{i\pi h/b})_{\mathbf{k}}$+c.c. have a larger scaling dimension than the cross terms, $(e^{-i\pi h/b})_{-\mathbf{k}}(e^{i\pi h/b})_{\mathbf{k}}$+c.c. Neglecting the former and expanding the latter, we arrive at the following stiffness correction:

$$\delta\mathcal{F} = -\frac{1}{2}\sum_{\mathbf{k}} J_k \kappa^* k^2 h_{-\mathbf{k}} h_{\mathbf{k}}, \tag{52}$$

where we introduced a nonlocal coupling $J_k \equiv 2B\lambda^2/|\mathbf{k}|$. Note that the screening length d does not contribute to the stiffness correction, affecting only the value of B. The negative sign of the stiffness correction (52) is consistent with the observed stiffness reduction in MC simulation with long-range interaction, compared to $\kappa_{\Delta\mathrm{IAFM}}$.

The coupling J is renormalized via integrating out the height fluctuations $h_{\mathbf{k}}$ with $1/l_1 < k < 1/l_0$,

$$J_{l_1^{-1}} = J_{l_0^{-1}} \left(\frac{l_1}{l_0}\right)^{1-4\kappa^*/\kappa}. \tag{53}$$

The stiffness correction (52) is relevant only when the condition (48) holds. Therefore, there is no qualitative effect on the Gaussian behavior (32).

We point out that the negative contribution to stiffness, Eq. (52), can be understood as an effect of long range interaction as follows. In the 3D cubic crystal picture, the charges of plus and minus sign reside on the even and odd sublattices. With respect to the (111) direction, used to introduce the height variable, these sublattices define alternating stacks of planes normal to the (111) axis, each filled with charges of one sign. Now, every surface with a small gradient of the height field can be associated with a set of terraces of alternating total charge and of width inversely proportional to the gradient of the height field. Since the long range Coulomb interaction favors the states with plus and minus charges well-mixed, one expects it to favor more narrow terraces compared to wider terraces. This means that the long range repulsive interaction contribution to the energetics of the height field must be negative of $(\nabla h)^2$, so that the favored states have the maximal possible height gradient. This observation is consistent with both the negative sign of the result (52) and with the stripe-like character of the ground state at $n = 1/2$ [Fig. 6(c), single domain], stabilized by the long-range repulsion.

C. Bounds on stiffness

To summarize the above results, the scaling relations set bounds on the effective stiffness κ in the freely fluctuating height model, Eq. (32). The Gaussian behavior is stable when the nonlinear terms are irrelevant, i.e., when

$$\kappa < \kappa_f < \kappa_g = \kappa_\lambda. \tag{54}$$

As the temperature decreases, the height surface becomes more rigid. There are several possible scenarios for a transition from a high-temperature (rough) to a low-temperature (smooth) phase. One is the fluctuation-driven roughening transition, involving the system freezing into a smooth phase due to the last term in (39) when κ approaches κ_f from below.[18,36]

Based on the evidence accumulated in our numerical simulations we conclude that such a behavior does not occur. We observe that the measured stiffness κ obeys the condition (54) as long as the height surface fluctuates appreciably. Hence, in particular, the coupling (40) to the gate voltage is irrelevant in the correlated phase of the model with the long-range interaction (2). This conclusion generalizes the observation[18] that the coupling to external field is irrelevant in the ΔIAFM (for sufficiently small field).

Lowering the temperature further produces a sharp freezing into a ground state in which the height surface does not fluctuate. While the freezing is accompanied by a steep increase of κ to immeasurably high values, the latter takes place at $T \approx T_c$. Due to narrow temperature interval in which this increase occurs, it is difficult to attribute it to the effect of height fluctuations. Instead, the observed behavior is consistent with an ordinary freezing by a first- or second-order phase transition (as discussed in Sec. III).

Above the freezing temperature, in the correlated phase the density and height fields effectively decouple, since the coupling λ is irrelevant. Indeed, the inequality (48) cannot be satisfied in the correlated phase, Eq. (54). This justifies *a posteriori* our phenomenological approach of including both the height and the density in the partition function (37). Similar arguments also explain why the negative correction (52) to the stiffness does not cause an instability. The latter would require $\kappa \geqslant \kappa_\lambda$, the condition forbidden in the correlated phase by Eq. (54).

Finally, the absence of the dislocation-unbinding phase transition between the correlated fluid and the high temperature disordered phase (studied in Sec. VII above) can also be understood based on the condition (54). Since $\kappa < \kappa_f < \kappa_{\mathrm{KT}}$, the lower bound (36) is never reached. (Similar argument was used in Ref. 34 for the ΔIAFM in zero or small external field.)

IX. DYNAMICS OF THE HEIGHT FIELD

The weakly coupled fluctuations of height and density in the correlated phase lead to interesting dynamical effects. Employing the Langevin dynamics, here we discuss how the interplay between the h and n fields affects the dynamical properties. We find the corrections to the conductivity and compressibility due to the height fluctuations, perturbative in the height-density coupling λ.

The nonconserving Langevin dynamics for the height field has the form

$$\partial_t h(\mathbf{r},t) = -\eta T \frac{\delta\mathcal{F}}{\delta h} + \xi_{\mathbf{r},t}, \tag{55}$$

with $\mathcal{F}$ given by Eq. (38), and ξ the stochastic force,

$$\langle \xi_{\mathbf{r},t} \xi_{\mathbf{r}',t'} \rangle = \langle \xi^2 \rangle \delta(t-t') \delta(\mathbf{r}-\mathbf{r}'). \tag{56}$$

Since the temperature T is included in $\mathcal{F}$, it multiplies the kinetic coefficient η in Eq. (55), so that the form of the

fluctuation-dissipation relationship is preserved,

$$\langle \xi^2 \rangle = 2\eta T. \tag{57}$$

The conserving Langevin dynamics for the charge density n is defined using the continuity equation

$$\partial_t n + \nabla_{\mathbf{r}} \mathbf{j} = 0, \quad \mathbf{j} = -\sigma T \nabla_{\mathbf{r}} \frac{\delta \mathcal{F}}{\delta n} + \mathbf{j}^L, \tag{58}$$

with the fluctuating extraneous part $\mathbf{j}^L$ obeying

$$\langle j_\mu^L(\mathbf{r},t) j_\nu^L(\mathbf{r}',t') \rangle = \langle (\mathbf{j}^L)^2 \rangle \delta_{\mu\nu} \delta(t-t') \delta(\mathbf{r}-\mathbf{r}'). \tag{59}$$

The conductivity σ is related to $\mathbf{j}^L$ variance by the Nyquist formula

$$\langle (\mathbf{j}^L)^2 \rangle = 2\sigma T. \tag{60}$$

Equations (55), (58), (39), (41), and (42) yield

$$\partial_t h(\mathbf{r},t) = \eta T \left(\kappa \nabla^2 h + \frac{2\pi g}{b} \sin \frac{2\pi h}{b} + \frac{\pi}{b} (\lambda n + f) \sin \frac{\pi h}{b} \right) + \xi(\mathbf{r},t), \tag{61}$$

$$\partial_t n(\mathbf{r},t) = \sigma T \nabla_{\mathbf{r}}^2 \left(\int d^2\mathbf{r}' U_{\mathbf{r}-\mathbf{r}'} n_{\mathbf{r}'} + \Phi_{\mathbf{r}}^{\text{ext}} \right) - \nabla_{\mathbf{r}} (\mathbf{j}^h + \mathbf{j}^L), \tag{62}$$

where we write the stochastic contribution to the current due to the height-field fluctuations in the form

$$\mathbf{j}^h(\mathbf{r},t) = -\lambda \sigma T \nabla_{\mathbf{r}} \cos \frac{\pi h_{\mathbf{r}}}{b}. \tag{63}$$

The height-field fluctuations provide an additional contribution $\delta\sigma^h$ to the conductivity, which is determined by the fluctuation-dissipation theorem,

$$\langle j_\mu^h(-\omega,-\mathbf{k}) j_\nu^h(\omega,\mathbf{k}) \rangle = 2\delta\sigma_{\mu\nu}^h(\omega,\mathbf{k}) T. \tag{64}$$

The contribution to the conductivity that arises from the height field fluctuations is purely longitudinal,

$$\delta\sigma_{\mu\nu}^h(\omega,\mathbf{k}) = \frac{\lambda^2 T}{2} \sigma^l(-\omega,-\mathbf{k}) \sigma^l(\omega,\mathbf{k}) k_\mu k_\nu \tilde{F}(\omega,\mathbf{k}). \tag{65}$$

Here $\sigma^l(\omega,\mathbf{k})$ is the longitudinal part of the total conductivity σ, and $\tilde{F}(\omega,\mathbf{k})$ is a Fourier transform of the correlator

$$F(\mathbf{r},t) = \left\langle \cos \frac{\pi h_{\mathbf{r},t}}{b} \cos \frac{\pi h_{0,0}}{b} \right\rangle_0 = \frac{1}{2} \exp\left\{ -\frac{\pi^2}{2b^2} \langle (h_{\mathbf{r},t} - h_{\mathbf{0},0})^2 \rangle_0 \right\}. \tag{66}$$

Averaging in (66) with respect to the Gaussian free energy, $\lambda = g = 0$ in Eq. (61), yields

$$\langle (h_{\mathbf{r},t} - h_{\mathbf{0},0})^2 \rangle_0 = \sum_{\mathbf{k},\omega} \frac{\langle \xi^2 \rangle}{(\eta T \kappa k^2)^2 + \omega^2} |1 - e^{i\mathbf{k}\mathbf{r} - i\omega t}|^2 = \frac{1}{\pi\kappa} \int_0^{1/a} dk \frac{1 - e^{-\eta\kappa k^2 |t|} J_0(kr)}{k}. \tag{67}$$

We are interested in the asymptotic behavior of the height correlator at large separation $r \gg a$. From the small k expansion under the integral (67) we have

$$1 - e^{-\eta\kappa k^2 |t|} J_0(kr) \sim k^2 \left(\frac{r^2}{4} + \eta\kappa |t| \right). \tag{68}$$

Therefore the height correlator (67) asymptotic behavior at $r \gg a$ is consistent with Eq. (35),

$$\langle (h_{\mathbf{r},t} - h_{\mathbf{0},0})^2 \rangle_0 \simeq \frac{1}{2\pi\kappa} \ln \left(\frac{\mathbf{r}^2}{4a^2} + \frac{\eta\kappa |t|}{a^2} \right). \tag{69}$$

At large r,t the correlation function (66), as well as the current $\mathbf{j}^h$ correlation (64) and (65), are thus of a power law form,

$$F(\mathbf{r},t) = \frac{1}{2} \left(\frac{a^2}{\mathbf{r}^2/4 + \eta\kappa |t|} \right)^{2\kappa^*/\kappa}. \tag{70}$$

With $\kappa < \kappa^*$ in the correlated phase, the function $F(\mathbf{r},t)$ rapidly decays at large spatial and temporal separations. We conclude from Eqs. (64), (65), and (70) that in this case the current $\mathbf{j}^h(\mathbf{r},t)$ space and time correlations have short memory and are local. Hence one may treat $\mathbf{j}^h(\mathbf{r},t)$ as an additional source of the Johnson-Nyquist noise, and our approach based on the fluctuation-dissipation theorem (64) is *a posteriori* justified.

Finally we consider the correction to the compressibility of the charged system due to the height fluctuations. It can be obtained directly from the statistical averaging with respect to the canonical distribution. The compressibility ν, defined as

$$\nu_{\mathbf{k}}^{-1} = \langle \Phi_{-\mathbf{k}} \Phi_{\mathbf{k}} \rangle, \quad \text{with } \Phi = \frac{\delta \mathcal{F}}{\delta n}, \tag{71}$$

acquires the perturbative correction as a result of the height-density coupling (42). The uniform ($k=0$) part $\delta\nu$ is obtained from

$$[\nu^{(0)} + \delta\nu]^{-1} = U_{\mathbf{k}=\mathbf{0}} + \delta U_{\mathbf{k}=\mathbf{0}}, \tag{72}$$

with the height field-induced density-density interaction

$$\delta U_{\mathbf{k}} = \lambda^2 \int d^2\mathbf{r} e^{-i\mathbf{k}\mathbf{r}} \left\langle \cos \frac{\pi h_{\mathbf{r}}}{b} \cos \frac{\pi h_{\mathbf{0}}}{b} \right\rangle_0. \tag{73}$$

The correlator (73) is given by Eq. (70) with $t=0$. Thus the compressibility correction due to fluctuations

$$\delta\nu = -\lambda^2 [U_{\mathbf{k}=0}]^{-2} \int d^2\mathbf{r} F(\mathbf{r}, t=0). \tag{74}$$

This correction is finite in the correlated phase. Indeed, the correlator in (73) is local when $\kappa < 2\kappa^*$ which is consistent

with the condition (54), and, thus, the integral in Eq. (74) is infrared convergent.

X. SUMMARY

In the present work we analyze the problem of charge ordering and dynamics of classical electrons on a 2D triangular array, by relating it to the better studied problem of the triangular Ising antiferromagnet. The phase diagram (Fig. 3) is found to be more rich than in the latter problem due to long-range electron interactions interplay with the geometrical frustration. At low temperatures, the electron system freezes into commensurate or disordered ground states in a continuous range of densities. We demonstrate that transport can be employed to study charge ordering, with the singularities of conductivity marking the phase transitions.

At intermediate temperatures, we idenitify the topological fluid phase characterized by strong electron correlations. The fluid state is described in terms of a nonlocal order parameter, the height field. We find that the short-range correlations in the charge system correspond to Gaussian fluctuations of the height field in the presence of topological defects. We determine numerically the effective stiffness of the height field, and rule out the Berezinskii-Kosterlits-Thouless phase transition, concluding that the topological defects remain unbound above freezing. In this phase the electron transport, resulting from short-range correlations enforcing local continuity of the height field, takes the form of "free" charge dynamics corresponding to height field fluctuations. We found that both the topological defects and the height fluctuations contribute to transport, their relative contribution depending on the concentration of the defects.

The ground state properties have been studied in this work for the simplest fractions $n=1/3,2/3$, and $n=1/2$. In transport, freezing is manifest by singularities in zero bias conductivity which drops to zero in the ordered phases. The sensitivity of transport to ordering of the electron system makes it a useful probe of 2D charge states.

While the situation at $n=1/3,2/3,1/2$ is fairly conventional, the precise nature of ordering for generic density remains unclear. Here several different scenarios can be anticipated. One is a devil's staircase of incompressible states at any rational n. In the relatively small system studied using MC dynamics, we have indeed found freezing into higher-order fractions with relatively small denominator, such as the "striped" $n=3/7$ state shown in Fig. 6(d). Similarly, other states with rational $n=p/q$ could become incompressible at low temerature, with T_c decreasing with the increase of the denominator q, forming the devil's staircase. Another possibility is the appearance, besides the simple rational fractions, of a family of disordered ground states. One documented example of such a behavior is the preroughening phenomenon[37] which describes a continuous phase transition into a disordered flat phase of a 3D crystal surface, characterized by the height surface with a disordered array of steps. The tunability of the form of interaction in the quantum dot arrays should allow to explore these, and other complex states.

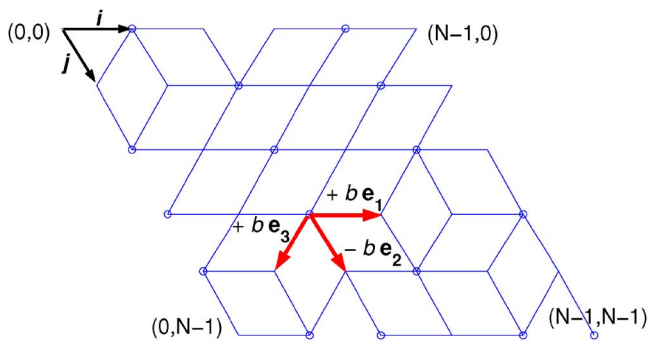

FIG. 10. (Color online) Assigning auxiliary 3D coordinates to the sites of the array.

ACKNOWLEDGMENTS

We are grateful to our colleagues Marc Kastner, Moungi Bawendi, and Nicole Morgan for drawing attention to this problem and for useful discussions. We thank Sergei Korshunov for insightful comments on the paper, and Pasquale Calabrese for a valuable discussion. The work at MIT was supported by the NSF MRSEC Grant No. DMR 02-13282. D.N. also acknowledges the NEC Grant for Advanced Materials (MIT), and support from NSF MRSEC Grant No. DMR 02-13706 (Princeton).

APPENDIX: ASSIGNING HEIGHT FIELD TO THE ARRAY

Here we describe the procedure by which the height values are assigned to the sites of the array. It should be noted that the height is well defined only at $T=0$, in the absence of topological defects, while at finite temperature it is defined only locally, in the regions away from the defects. As we found in Sec. V, the defects are always present in the correlated phase, since there is no defect binding phase transition. This complication, however, is inessential, since the number of defects is exponentially small at low enough temperature, and is often zero for the finite patch used in our simulation. We found that defining the height locally in a system with a small number of defects does not lead to any significant errors in the statistics of fluctuations and, in particular, does not affect the numerical value of the effective stiffness κ.

We work with an $N\times N$ rhombic patch of the 2D triangular array, using the coordinate system aligned with the array, as shown in Fig. 10. The sites are labeled by integer coordinates (i,j), $i,j=0,\ldots,N-1$. We place the origin in the upper left-hand corner of the patch. The first component, i, is the site number counted along the horizontal axis (the patch upper edge). The numbers i increase as we go from left to right. The second component, j, is the site number along the axis which points downward and to the right at the angle $\pi/3$ with the horizontal axis. The numbers j increase as we go from the origin down and to the right, with $j=N-1$ at the lower edge of the patch. The conventional Cartesian coordinates $\mathbf{r}_m=(x_m,y_m)$ of the site (i_m,j_m) are given by

$$x_m = i_m a + j_m \frac{a}{2}, \quad y_m = -j_m a \frac{\sqrt{3}}{2}. \tag{A1}$$

To calculate the height $h(\mathbf{r}_m)$ for each point $\mathbf{r}_m=(x_m,y_m)$ we first assign the auxiliary 3D coordinates

$$\mathbf{R}(\mathbf{r}_m) = \sum_s R_s(\mathbf{r}_m)\mathbf{e}_s. \quad \text{(A2)}$$

Here the unit vectors $\mathbf{e}_s$, $s=1,2,3$, are the basis vectors of the auxiliary 3D simple cubic lattice.

To obtain the 3D coordinates $\mathbf{R}(i,j)$ for a particular charge configuration, we start from the upper left-hand corner, $\mathbf{R}(i=0,j=0)\equiv\mathbf{0}$, and assign the coordinates by the sequence of steps. We shall call the sites (i,j) and (i',j') *connected*, if the charges at these sites are opposite, i.e., the bond between these sites is not frustrated (and hence is drawn in Fig. 10).

To assign the height, we move from point to point in each row, $i=0,\ldots,N-1$, with j fixed, repeating it for all $j=0,\ldots,N-1$. Suppose that the heights of all the sites with $i'\leqslant i$ and $j'\leqslant j$ are already defined. The heights of the remaining one, two, or three sites that are connected to (i,j) are defined by the following rules (Fig. 10):

(i) If the site $(i+1,j)$ is connected to (i,j), then $R_1(i+1,j)=R_1(i,j)+b$;

(ii) If the site $(i,j+1)$ is connected to (i,j), then $R_2(i,j+1)=R_2(i,j)-b$;

(iii) If the site $(i-1,j+1)$ is connected to (i,j), then $R_3(i-1,j+1)=R_3(i,j)+b$, with b given by Eq. (24).

Once the 3D coordinates $\mathbf{R}(\mathbf{r}_m)$ are defined, the height at each site $\mathbf{r}_m$ is obtained by projecting onto the (111) crystal direction:

$$h(\mathbf{r}_m) = \sum_{s=1}^{3} R_s(\mathbf{r}_m). \quad \text{(A3)}$$

We note that for this procedure to work, each site must be connected, in the above sense, to at least one neighbor. Thus the height assignment may be impossible for charge configurations with very low density of unfrustrated bonds. However, at low enough temperatures, in the correlated fluid phase, at $n\simeq 1/2$, we do not encounter such configurations in our simulation.

Also, in the presence of defects, the above recipe assigns heights unambiguously, albeit in a somewhat *ad hoc* way. We do not explicitly exclude the configurations with defects from the height statistics analysis. Instead, we estimate their relative contribution (see Sec. VI) and find it to be small enough for the results (the stiffness value) to be affected.

*Electronic address: dima@alum.mit.edu

[1] A. P. Ramirez, Annu. Rev. Mater. Sci. **24**, 453 (1994).

[2] J. E. Mooij and G. Schön, in *Single Charge Tunneling*, edited by H. Grabert and M. H. Devoret (Plenum, New York, 1992), Chap. 8, and references therein; Physica B & C **142**, 1 (1988); H. S. J. van der Zant, W. J. Elion, L. J. Geerligs, and J. E. Mooij, Phys. Rev. B **54**, 10081 (1996); A. van Oudenaarden and J. E. Mooij, Phys. Rev. Lett. **76**, 4947 (1996); R. S. Newrock, C. J. Lobb, U. Geigenmüller, and M. Octavio, in *Solid State Physics*, edited by H. Ehrenreich and F. Spaepen (Academic, San Diego, 2000), Vol. 54, p. 263; P. Martinoli and Ch. Leemann, J. Low Temp. Phys. **118**, 699 (2000); R. Fazio and H. J. S. van der Zant, Phys. Rep. **355**, 235 (2001).

[3] D. Heitmann and J. P. Kotthaus, Phys. Today **46**(1), 56 (1993); H. Z. Xu *et al.*, J. Cryst. Growth **206**, 279 (1999), **205**, 481 (1999).

[4] S. Teitel and C. Jayaprakash, Phys. Rev. Lett. **51**, 1999 (1983); T. C. Halsey, J. Phys. C **18**, 2437 (1985); S. E. Korshunov and G. V. Uimin, J. Stat. Phys. **43**, 1 (1986); S. E. Korshunov, *ibid.* **43**, 17 (1986); E. Granato, J. M. Kosterlitz, J. Lee, and M. P. Nightingale, Phys. Rev. Lett. **66**, 1090 (1991); J.-R. Lee and S. Teitel, Phys. Rev. Lett. **66**, 2100 (1991).

[5] S. E. Korshunov, Phys. Rev. B **63**, 134503 (2001); L. B. Ioffe and M. V. Feigel'man, *ibid.* **66**, 224503 (2002); B. Douçot, M. V. Feigel'man, and L. B. Ioffe, Phys. Rev. Lett. **90**, 107003 (2003); V. Cataudella and R. Fazio, Europhys. Lett. **61**, 341 (2003); S. E. Korshunov, Phys. Rev. Lett. **88**, 167007 (2002); Phys. Rev. B **71**, 174501 (2005).

[6] K. Takada, H. Sakurai, E. Takayama-Muromachi, F. Izumi, R. A. Dilanian, and T. Sasaki, Nature (London) **422**, 53 (2003).

[7] A. I. Yakimov *et al.*, J. Phys.: Condens. Matter **11**, 9715 (1999); Phys. Low-Dimens. Semicond. Struct. **3–4**, 99 (1999); E. Ribeiro, E. Muller, T. Heinzel, H. Auderset, K. Ensslin, G. Medeiros-Ribeiro, and P. M. Petroff, Phys. Rev. B **58**, 1506 (1998).

[8] A. Groshev and G. Schön, Physica B **189**, 157 (1993); T. Takagahara, Optoelectron., Devices Technol. **8**, 545 (1993); Surf. Sci. **267**, 310 (1992); G. Medeiros-Ribeiro, F. G. Pikus, P. M. Petroff, and A. L. Efros, Phys. Rev. B **55**, 1568 (1997); O. Heller, P. Lelong, and G. Bastard, Physica B **251**, 271 (1998).

[9] C. B. Murray, C. R. Kagan, and M. G. Bawendi, Science **270**, 1335 (1995); C. B. Murray, D. J. Norris, and M. G. Bawendi, J. Am. Chem. Soc. **115**, 8706 (1993).

[10] C. A. Leatherdale, C. R. Kagan, N. Y. Morgan, S. A. Empedocles, M. A. Kastner, and M. G. Bawendi, Phys. Rev. B **62**, 2669 (2000).

[11] N. Y. Morgan, C. A. Leatherdale, M. Drndic, M. V. Jarosz, M. A. Kastner, and M. G. Bawendi, Phys. Rev. B **66**, 075339 (2002); M. Drndic, M. V. Jarosz, N. Y. Morgan, M. A. Kastner, and M. Bawendi, J. Appl. Phys. **92**, 7498 (2002).

[12] M. den Nijs, in *Phase Transitions and Critical Phenomena*, edited by C. Domb and J. Lebowitz (Academic, London, 1988), Vol. 12.

[13] K. Kawasaki, Phys. Rev. **148**, 375 (1966); in *Phase Transitions and Critical Phenomena*, edited by C. Domb and M. S. Green (Academic, London, 1972), Vol. 2.

[14] R. J. Glauber, J. Math. Phys. **4**, 294 (1963).

[15] P. C. Hohenberg and B. I. Halperin, Rev. Mod. Phys. **49**, 435 (1977).

[16] G. H. Wannier, Phys. Rev. **79**, 357 (1950); J. Stephenson, J. Math. Phys. **5**, 1009 (1964); J. Math. Phys. **11**, 413 (1970).

[17] H. W. J. Blöte and H. J. Hilhorst, J. Phys. A **15**, L631 (1982).

[18] B. Nienhuis, H. J. Hilhorst, and H. W. J. Blöte, J. Phys. A **17**, 3559 (1984).

[19] R. J. Baxter, *Exactly Solved Models in Statistical Mechanics* (Academic, New York, 1982).

[20] E. Domany, M. Schick, J. S. Walker, and R. B. Griffiths, Phys. Rev. B **18**, 2209 (1978); E. Domany and M. Schick, *ibid.* **20**, 3828 (1979).
[21] C. Rottman, Phys. Rev. B **24**, 1482 (1981).
[22] L. D. Landau and E. M. Lifshits, *Statistical Physics, Part I* (Pergamon, New York, 1969).
[23] D. S. Novikov and L. S. Levitov (unpublished).
[24] J. K. Kjems, L. Passell, H. Taub, J. G. Dash, and A. D. Novaco, Phys. Rev. B **13**, 1446 (1976).
[25] E. Domany and E. K. Riedel, Phys. Rev. Lett. **40**, 561 (1978).
[26] H. Pfnür and P. Piercy, Phys. Rev. B **41**, 582 (1990); L. D. Roelofs and C. Jackson, *ibid.* **47**, 197 (1993).
[27] P. Calabrese, E. V. Orlov, D. V. Pakhnin, and A. I. Sokolov, Phys. Rev. B **70**, 094425 (2004).
[28] S. E. Korshunov, Phys. Rev. B **72**, 144417 (2005).
[29] *M. C. Escher: The Graphic Work* (Taschen, Cologne, 1992).
[30] C. Zeng and C. L. Henley, Phys. Rev. B **55**, 14935 (1997).
[31] H. Yin, B. Chakraborty, and N. Gross, Phys. Rev. E **61**, 6426 (2000).
[32] V. L. Berezinskii, Sov. Phys. JETP **32**, 493 (1971); J. M. Kosterlitz and D. J. Thouless, J. Phys. C **6**, 1181 (1973); J. M. Kosterlitz, *ibid.* **7**, 1046 (1974).
[33] B. I. Halperin and D. R. Nelson, Phys. Rev. Lett. **41**, 121 (1978); A. P. Young, Phys. Rev. B **19**, 1855 (1979).
[34] H. W. J. Blöte, M. P. Nightingale, X. N. Wu, and A. Hoogland, Phys. Rev. B **43**, 8751 (1991).
[35] P. Chandra, P. Coleman, and L. B. Ioffe, Phys. Rev. B **49**, 12897 (1994).
[36] J. D. Weeks, *Ordering in Strongly Fluctuating Condensed Matter Systems*, edited by T. Riste (Plenum, New York, 1980).
[37] K. Rommelse and M. den Nijs, Phys. Rev. Lett. **59**, 2578 (1987).